Author Version: Journal of Asian Earth Sciences, vol.157; 2018; 187-197

Paleomagnetic record for the past 80 ka from the Mahanadi basin, Bay of Bengal

Usapkar, A., Dewangan, P*., Mazumdar, A., Krishna, K.S., Ramprasad, T., , Badesab, F.K. Patil, M., Virsen, G. V.

CSIR-National Institute of Oceanography, Dona-Paula, Goa 403004, India.

*corresponding author email: pdewangan@nio.org

Abstract

High resolution paleomagnetic investigations were performed on a 50.08 m long sediment core (MD161/20) from Mahanadi basin, Bay of Bengal. Core yielded reliable paleomagnetic results for top 20 meter below seafloor (mbsf) which spans about 80 ka. Based on the analysis of rock magnetic data, the core is subdivided in to five distinct Zones: Zone 1 and Zone 2 cover top 20 mbsf and do not show any abrupt change in magnetic mineralogy, concentration and grain size. Zones 3 and 5 show significant reduction in χ_{LF}, χ_{ARM} and SIRM due to dissolution of magnetic minerals. Zone 4 shows moderate values of χ_{LF} and SIRM. The low value of χ_{ARM} suggests that magnetic signal is mostly carried by magnetic grains in PSD/MD state. The paleomagnetic data for the top 20 mbsf show four prominent geomagnetic excursions at ~9 mbsf, ~13.5-15 mbsf, ~16.3 mbsf and ~18-18.2 mbsf. The age-depth relationship is established using stratigraphic correlation between well-dated sedimentary core NGHP-01-19B and the core MD161/20. The ages of the observed excursions correspond to ~18-20 ka, ~42-49 ka, ~54-57 ka and ~69-70 ka. The excursions at ~42-49 ka, ~54-57 ka, and ~67-70 ka is similar to the known excursions the Laschamp and the split Norwegian-Greenland Sea events (NGS-I and NGS-II). The excursion at 18-20 ka is not observed globally and may be related to lithological/sedimentological changes occurring during last glacial maxima (LGM). The virtual geomagnetic path (VGP) of Laschamp excursion traces clockwise loop. All excursions identified in present study fall in the periods of relatively low paleointensity.

Keywords: Magnetic stratigraphy, paleomagnetic excursions, Laschamp event, Norwegian-Greenland Sea events, virtual geomagnetic path

Introduction

Magnetostratigraphy is a powerful tool for stratigraphic correlations. Paleomagnetic investigations are gaining importance globally to study the variation of the Earth's magnetic field for refining the magnetic polarity time scale that can be used effectively for stratigraphic correlation and understanding the geodynamo processes of the Earth's magnetic field (Hanna and Verosub, 1989, Gubbins, 1991). Depending on the timescale, the Earth's magnetic field shows three types of behaviours: geomagnetic secular variation (10^2-10^3 years), geomagnetic excursions (10^3-10^4 years) and geomagnetic reversals (10^5-10^6 years). Records of geomagnetic secular variation and geomagnetic reversals are relatively well documented; however, the record of geomagnetic excursions are not been firmly established due to the complexity associated with the identification of geomagnetic excursions. Geomagnetic excursions are short lived events which can help in improving the paleomagnetic stratigraphy, especially during Brunhes chron. Geomagnetic excursions may represent high amplitude secular variation, aborted reversal or a reversal of short duration (Verosub, 1982) and may serve as a potential chronostratigraphic marker. During a geomagnetic excursion, large fluctuation in the paleomagnetic direction and intensity is expected within a short duration. However, identification and use of geomagnetic excursion in magnetostratigraphy still remain highly debatable and controversial (Verosub and Banerjee, 1977). The limiting factors are the spatial and temporal behaviour of the excursions, precise determination of paleomagnetic signal and age/chronology associated with the excursions. Mostly, ambiguity arises in correlating the paleomagnetic signature at geographically different sites with same chronology.Further, diagenetic complications due to reductive dissolution of magnetic iron oxides and authigenic growth of iron sulfides (Dekkers et al., 1994) may destroy the primary NRM signal or delay the NRM acquisition (Van Hoof et al., 1993) resulting in partial or total eradication of paleomagnetic excursions. Sometimes alteration of existing magnetic minerals may also lead to spurious magnetization directions (Heider and Dunlop, 1987).Numerous excursions during Brunhes chron such as Monolake (Liddicoat and Coe, 1979; Negrini et al., 1984), Laschamp (Bonhommet and Zahringer, 1969; Bonhommet and Babkine, 1967; Levi et al., 1990); Norwegian-Greenland (O'Regan et al., 2008; Channell and Xuan, 2009); Blake (Smith and Foster, 1969; Tucholka et al., 1987; Tric et al., 1991; Zhu et al., 1994). The Pringle Falls (Herrero-Bervera et al., 1989; Herrero-Bervera et al., 1994) and Biglost excursions (Negrini et al., 1987; D.E. Champion et al., 1988)

are identified across the globe. Most of these excursions are identified at higher latitudes and clustered around Europe, America and Northern and Central Asia. There are not many secular variation records of geomagnetic excursions from low latitude regions and in particular from Bay of Bengal where high resolution, continuous sediment repository is available.

Therefore, the core MD161/20 (length= 50.08 m, Latitude= 18 47.3598´N and Longitude= 85 36.4373´E), collected in the Mahanadi basin, Bay of Bengal at a water depth of 1866 m, (**Fig. 1**) is studied to reconstruct the magnetostratigraphy. In the present study, we constructed Paleosecular variation (PSV) record for top 38 mbsf for the core MD161/20. The PSV record of top 20 mbsf is reliable with a very good chronology. The PSV records beyond 20 mbsf are not reliable and were obtained either at demagnetization step of 20 mT or 15 mT. This limits our ability to identify any excursions occurring beyond 80 ka i.e., below 20 mbsf.

2. Geology of the study area.

Mahanadi basin is a passive pericratonic rift and a potential petroliferous basin situated along the eastern continental margin of India. The basin extends from 19° 27´ to 23°35´N and 80°30´ to 86°50´E covering an area of 260,000 km^2 (Singh 2008). Mahanadi basin was formed due to rifting of Gondwanaland during Jurassic period (Rao et al., 1997; Sastri et al., 1981; Subrahmanayam et al., 2008) and the geology of the basin is predominantly characterized by Precambrian rocks of the Eastern Ghats consisting of khondolites, charnokites, leptynites, granites gneisses, rocks associated with the Gondwana supercontinent such as limestone, shales and sandstones and recent littoral deposits (Chakrapani and Subramanian 1993). Most of the detrital input to the basin is brought by river Mahanadi and its tributaries Shaonath, Jonk, Harado, Mand, Ib, Tel and Ong. The analysis of the suspended load shows the presence of Kaolinite, Chlorite, Quartz and Dolomite (Chakrapani and Subramanian, 1990; Subramanian, 1980). The major clay minerals in the Mahanadi basin are Ilite (23-64 %) followed by Smectite (9.6-53.6 %) (Mazumdar et al., 2015). The basin is overlain by sedimentary and volcanic sequences from Cretaceous to Recent. The basin forms a part of richest mineral belt of iron ore, coal, limestone, dolomite, bauxite, lead and copper (Chakrapani and Subramanian, 1993).

3. Methods and data sets

The Mahanadi basin core MD161/20 recovered on board *D/V Marion Dufresne* was cut into 1.5 m sections and further split into two halves with respect to fixed reference line marked along the length of the core liner. The sections were subsampled at a resolution of 5 cm using 7 cm^3 cylindrical vials to carry out paleomagnetic investigations. A total of 35 sections were subsampled and 939 samples were analysed for paleomagnetic studies. The orientation of the sub-samples was preserved with respect to the reference line pre-marked along the core liner. Natural remanent magnetization (NRM) was measured prior to any induced field laboratory treatment on all discrete samples using Molspin fluxgate spinner magnetometer. Two pilot samples from each of the section were selected and were progressively demagnetized using AF-Demagnetizer from 0 to 100 mT in steps of 5 mT. Pilot samples suggest that the dominant portion of viscous component of magnetization is erased within demag steps of 10 mT to 15 mT, and demag steps from 15 mT to 45 mT reveal stable component of remanent magnetization (ChRM). Based on the results of these pilot samples, remaining samples were demagnetized from 0 to 70 mT in steps of 10 mT. The characteristic remanent magnetisation (ChRM) i.e., paleomagnetic inclination, declination, intensity and maximum angular deviation (MAD) is calculated using principal component analysis using least square method (Kirschvink, 1980). The information regarding direction and magnitude of NRM vector after each demagnetization step was represented using orthogonal representation of Zijderveld diagram also known as vector end plot diagram.

To test the stability of paleomagnetic records, rock magnetic measurements were carried on wet samples of MD161/20 at a resolution of 5 cm. Magnetic susceptibility was measured using Bartington MS2B dual frequency susceptibility meter. Susceptibility measurements were done at two frequencies χ_{LF}= 0.47 kHz and χ_{HF}= 4.7 kHz and its frequency dependent susceptibility was computed as per formula $\chi_{FD}\% = (\chi_{LF}-\chi_{HF})/\chi_{LF} \times 100$. Anhysteric remanent magnetization (ARM) was measured using AF-Demagnetizer with p-ARM attachment, 100 mT AF field was superimposed on a fixed DC bias field of 50 µT. Susceptibility of ARM i.e., χ_{ARM} is computed as mass normalized ARM divided by DC bias field. Isothermal remanent magnetization (IRM) was imparted using Molspin MMP10 pulse magnetizer. IRM fields imparted to the samples are as follows: 1T in forward direction and -20 mT, -30 mT, -100 mT and -300 mT in backward direction. Saturation isothermal remanent magnetization (SIRM) is computed as mass normalized SIRM acquired at a peak field of 1 T. S-ratio was calculated as S-ratio= IRM_{300mT}/IRM_{1T} (Thompson and Oldfield, 1986; Bloemendal et al., 1988). Soft-IRM and

Hard-IRM (HIRM) was calculated using the formulae [Soft-IRM= (IRM_{1T}+IRM_{-30mT})/2] and [HIRM= (IRM_{1T}+$IRM_{.300mT}$)/2] (Liu et al., 2007).

The magnetic particles were separated from the bulk sediment samples from the selected depths of 2.0, 8.5, 10.95, 13.45, and 15.95 mbsf following the method of Petersen et al. (1986). The magnetic separates were analyzed using a scanning electron microscope (JEOL JSM-IT 300) to capture high resolution images of the magnetic grains. The energy dispersive energy dispersive X-ray spectroscopy (EDS) probe attached to the microscope was used to perform elemental analysis on magnetic separates and to infer the magnetic mineralogy.

4. Paleomagnetic Results

The Zijderveld plot for selected samples of core MD161/20 shows that the stable component of characteristic remanent magnetization (ChRM) can be obtained beyond 15 mT (**Fig. 2A, B**). The viscous remanence magnetization are mostly eliminated by applying demag fields of 5 to 10 mT, and the stable component data of the remanence magnetization (ChRM) is obtained between the demag field of 15 and 45 mT. The results of stepwise AF demagnetization are plotted and analysed using Zijderveld diagrams (Zijderveld, 1967) also known as vector end plot diagrams. ChRM information is extracted from orthogonal projection of Zijderveld diagram using least square analysis (Kirschvink, 1980). The ChRM paleoinclination as well as the paleoinclination obtained at 20mT is shown with respect to depth in **Fig. 3A** . Paleoinclination values at ChRM and 20 mT are similar for the top 20 mbsf suggesting negligible effect of viscous remanent magnetization at 20 mT. Paleoinclination values for top 13.5 mbsf fluctuate between 20° and 70° except at a very short interval at 9 mbsf where it swings to -60°. We also see a prominent band of negative inclination between 13.5 and 15 mbsf, and beyond that depth several low-amplitude fluctuations in inclination is observed. A sharp decrease in inclination followed by a rapid increase in inclination is observed at 16.3 mbsf showing typical characteristics of geomagnetic excursion. Further, a very short duration of negative paleoinclination is observed between 18 and 18.2 mbsf. ChRM can be estimated with reasonable confidence for the uppermost 20 mbsf; however, below this depth the ChRM cannot be estimated due to drop in NRM intensity. Maximum angular deviation (MAD) is shown in **Fig. 3D**. For top 20 mbsf, the average MAD is about 4, except at two locations ~1.5 mbsf and between 12.5 and 13.5 mbsf, where it increases to

~10-12. ChRM data and the data obtained at 20 mT demagnetization step show one to one correlation suggesting a negligible effect of viscous remanent magnetization. Several excursions are identified in the paleomagnetic records which can be correlated with the known events in Brunhes chron such as Mono Lake (27-28 ka BP: Denham & Cox 1971; Liddicoat & Coe 1979 and 33-36 ka BP: Kissel et al., 2011), Laschamp (42 ka BP: Bonhomet and babkine 1967; Levi et al. 1990) and the split Norwegian-Greenland Sea events (55 and 66 ka BP: Langereis et al., 1997, Nowaczyk and Baumann, 1992; Nowaczyk and Frederichs, 1999). Beyond 20 mbsf, we could not retrieve reliable PSV records due to a sudden drop in NRM intensity. Paleoinclination and paleodeclination data below 20 mbsf are too noisy and show large scatter in direction; MAD also shows large scatter, and increase to 10-20. Therefore, the ChRM data below 20 mbsf are not interpreted in the present study.

Paleodeclination is relative and is obtained by subtracting an arbitrary constant from the observed declination data (**Fig. 3B**) such that the mean declination data of the shallow sediments is close to the present day declination at this site. Relative paleodeclination varies between ~-140° to ~160° for top 20 mbsf. Rapid fluctuations observed below 20 mbsf are probably associated with low paleointensity. A minor upward swing is observed in paleodeclination at ~9 mbsf and in the vicinity of 13.5-15 mbsf. A minor downward swing is observed in paleodeclination in the vicinity of 16.3 mbsf and between 18-18.2 mbsf.

Relative paleointensity (**Fig. 3C**) is obtained by normalizing NRM intensity obtained at 20 mT demagnetization step by both susceptibility and SIRM. Paleointensity mostly fluctuates between 2 and 7 for the top 20 mbsf. We see a slight drop in paleointensity in the vicinity of the observed paleoinclination anomaly at 13.5-15 mbsf, 16.3 mbsf and 18-18.2 mbsf. However, we did not observe any anomaly in paleointensity in the vicinity of 9 mbsf paleoinclination anomaly. NRM intensity of samples below 20 mbsf is very low, and directional data are randomized within 10 to 15 mT demag step. The paleomagnetic data are listed in Table 1 at an interval of 50 cm, and the complete data is available as a supplementary material.

5. Rock magnetic results

Rock magnetic data is obtained for the core MD161/20 to assess the stability of paleomagnetic records and to identify regions of anomalous magnetic parameters, if any. The magnetic parameters χ_{LF}, χ_{ARM} and SIRM (**Fig. 4A**) show a similar pattern and can be categorized in five different zones (Zone 1- Zone 5). The magnetic parameters in Zone 1 show a broad oscillation with a minimum at 5

mbsf. Large amplitude, high-frequency variation is observed in Zone 2 for χ_{LF}, χ_{ARM} and SIRM. Significantly reduced values for χ_{LF} and SIRM are observed in Zone 3. These parameters are sensitive to the concentration of magnetic minerals and also to magnetic grains in MD state (Dunlop 1973; Bailey and Dunlop 1983; Thompson and Oldfield 1986). In particular χ_{ARM}, parameter sensitive to stable single domain (SSD) magnetic grains, is almost negligible in this zone indicating a minor abundance of remanent carrying stable single domain (SSD)/PSD grains. A downcore increase in χ_{LF}, χ_{ARM} and SIRM is observed in Zone 4 and further below in Zone 5, all three parameters reduce to smaller values. The χ_{FD}% **(Fig. 4B),** a parameter sensitive to magnetic grains in superparamagnetic (SP) grain size range (Maher, 1988; Oldfield and Yu, 1994; Walden et al., 1999), is highly fluctuating and varies between 1 and 11. The running mean (5 pt average) represents the mean variations in χ_{FD}% and shows a minor increase in SP size grains in Zone 3. The χ_{ARM}/SIRM **(Fig 4B),** parameter sensitive to the remanent carrying stable single domain (SSD)/PSD grains (Maher, 1988), varies between 0.001-0.0024 mA^{-1} for the top 20 mbsf. However, it drops down drastically to ~0.0002-0.0004 mA^{-1} below 20 mbsf. The χ_{ARM}/SIRM ratio varies inversely with magnetic grain size (Maher and Taylor, 1988); higher values indicate finer magnetic grain size (SSD, PSD) and lower values correspond to coarse grains (MD). The abrupt drop of χ_{ARM}/SIRM values below 20 mbsf (average 0.0002) suggests the decrease in the abundance of SSD/PSD sized magnetic grains in Zone 3-Zone 5. The SIRM/χ_{LF} **(Fig. 4B)** ratio, a parameter sensitive to magnetic grains in PSD range (Tauxe, 1993), is uniform about (~ 12-14 Am^{-1}) for top 20 mbsf and abruptly decreases to ~2 Am^{-1} in Zone 3 with a minor exception in depth range 21.5-22.5 mbsf. The decrease in SIRM/χ_{LF} values suggests the decrease in the PSD sized magnetic grains in Zones 3 to 5. The SIRM/χ_{LF} ratio again increases in Zone 4, thereafter, the values drop down and fluctuate around 2- 4 Am^{-1}. The Soft-IRM and HIRM parameter values are sensitive to magnetically soft and hard coercivity minerals, respectively (Walden et al., 1999, Oldfield and Yu 1994). Soft-IRM shows relatively high values in Zone 2 and Zone 4 as compared to other zones indicating the presence of soft-magnetic minerals like magnetite/titanomagnetite in these zones. HIRM also shows higher values in Zone 2 and Zone 4 (**Fig. 4C**) suggesting a higher abundance of high-coercivity minerals like hematite/titanohematite. The S-ratio (**Fig. 4C**) is uniform, very close to unity for Zone 1, Zone 2 and Zone 4 indicating higher abundance of soft-magnetic mineral like magnetite/titanomagnetite as compared to hard-magnetic minerals like hematite/titanohematite (Thompson and Oldfield, 1986; Bloemendal et al., 1992; St-Onge et al., 2003; Heslop, 2009). In Zones

3 and 5, the S-ratio decreases slightly suggesting a relative increase in high coercivity magnetic minerals like hematite/titanohematite. The rock magnetic data are listed in Table 2 at an interval of 50 cm, and the complete data is available as a supplementary material.

The SEM images and EDS spectrum of magnetic minerals from different depth intervals are shown in **Fig. 5A-E.** Ferri-magnetic iron oxide minerals of different shapes and sizes are observed in the magnetic extract. In zone -1 (at 2.0 mbsf), the EDS data show the presence of iron with minor traces of titanium, manganese, calcium, silicon, aluminum and phosphorous (**Fig. 5A**). The EDS result of magnetic extracts from zone - 2 (8.5 and 15.95 mbsf) shows the presence of iron with higher Ti-content along with minor traces of manganese, vanadium, calcium, potassium, aluminum and silicon (**Fig. 5B,E**). The EDS analysis of the magnetic extracts within the inclination anomaly (at 13.45 mbsf) and outside the anomaly (at 10.95 mbsf) shows the octahedral magnetite/titanomagnetite grain with traces of titanium, calcium, potassium and aluminum (**Fig. 5C, D**).

6. Discussion

6.1 Stability of paleomagnetic record

A good reliable PSV record is carried by magnetic minerals of detrital origin in SSD/PSD state. A paleosecular variation record for top 20 mbsf i.e., for Zone 1 and Zone 2 does not show large scatter in direction, and MAD is low (averaging around 5). The rock magnetic parameters χ_{LF}, χ_{ARM} and SIRM also do not show any abrupt change in magnetic mineralogy, concentration and grain size within Zones 1 and 2 (**Fig. 4A**) suggesting that the paleomagnetic signal in Zone 1 and Zone 2 is mostly governed by magnetic minerals of detrital origin. The EDS analysis of the magnetic extracts shows that the magnetic mineralogy is mostly dominated by magnetite/hematite in Zone 1 and titanomagnetite/titanohematite with varying Ti-content in Zone 2. A similar increase in Ti/Fe ratio beyond 15 ka is also observed from the XRF data in the core NGHP-01-19B (Phillips et al., 2014). High χ_{ARM} values for Zone 1 and Zone 2 suggests the abundance of remanence carrying magnetic minerals in SSD/PSD domain magnetic grain size. The S-ratio for Zone 1 and Zone 2 is very close to unity suggesting that the paleomagnetic signal in Zone 1 and Zone 2 is dominantly carried by soft-magnetic mineral like magnetite/titanomagnetite (Thompson and Oldfield, 1986; Bloemendal et al., 1992; St-Onge et al; 2003; Heslop 2009). Further, the high values of Soft-IRM and HIRM in Zones 1 and 2 also suggest a higher abundance of remanent carrying soft and hard magnetic minerals. High

values of χ_{ARM}/SIRM and SIRM/χ_{LF} also support that remanence in these zones is mostly carried by SSD/PSD size magnetic grains (Maher, 1988; Dunlop and Xu 1994, Dunlop 1997). Thus, the PSV records from Zone 1 and Zone 2 (< 20 mbsf) are reliable for paleomagnetic interpretation. In contrast, Zone 3 and 5 show the reduction in χ_{LF}, SIRM and a significant reduction in χ_{ARM} suggesting that these zones have undergone extensive dissolution probably due to diagenesis. Low values of χ_{ARM}/SIRM and SIRM/χ_{LF} for Zone 3 and 5 suggest coarsening of magnetic grains, and S-ratio also deviates from unity indicating the presence of high coercive magnetic minerals. No reliable ChRM data is obtained for Zone 3 as the directional data are randomized within 10-15 mT demag steps. Therefore, the PSV record for this Zone comprises of the result from demagnetization step of 20 mT, and it showed large scatter in directions for 24.5-27.5 mbsf in Zone 3. No paleomagnetic data was retrieved in Zone 5 due to drastic drop in paleointensity signal to negligible values. The PSV data shown in **Fig. 3** for Zone 4 is either at demagnetization step of 20 mT or very few demagnetization steps. Data shows large scatter in direction and paleointensity is also very low. Rock magnetic parameters in Zone 4 depict moderate χ_{LF} and SIRM values and low χ_{ARM} values, suggesting that the magnetic signal in this zone is mostly carried by magnetic grains in PSD/MD state. Therefore, the data from Zone 4 should be interpreted with caution. Overall, the stability analysis suggests that the paleomagnetic signal is reliable for Zones 1 and 2 (< 20mbsf) and poor for Zones 3-5 (> 20 mbsf).

6.2 Chronology for the core MD161/20

One of the important requirements for the magnetostratigraphy is the precise age determination. The age-depth model for MD161/20 is constructed by establishing the stratigraphic correlation between well-dated sedimentary core NGHP-01-19B (Phillips et al., 2014) and MD161/20. We also compare the estimated age-depth curve of MD161/20 with another independent core MD161/19 (Mazumdar et al., 2014) for the shallow sediments. The cores NGHP-01-19B and MD161/19 are co-located (Latitude: 18° 59.1092´N, Longitude: 85º 41.1669´E), and they are separated from the core MD161/20 (Latitude: 18º 47.3598´N, Longitude: 85º 36.4373´E) by ~14 km. Phillips et al. (2014) established the chronology for the core NGHP-01-19B (Site 19) using both radiocarbon ages and oxygen isotope events from the benthic *Uvigerina peregrine* $\delta^{18}O$ record. Mazumdar et al. (2014) established the chronology for the shallow part of the core MD161/19 (up to 7 mbsf) using radiocarbon dating of the planktonic foraminifera species *Globigerina ruber* and *Globigerina sacculifer*. The Toba ash bed layer is identified on all the three cores (MD161/19 at depth 9.05 mbsf, MD161/20 at depth 19.05 mbsf, and

NGHP-01-19B at depth 8.44 mbsf), and is dated to be ~74 ky BP (Ninkovitch, 1979; Acharyya and Basu, 1993). Further, the Toba ash layer fits closely with the established chronology of cores NGHP-01-19B and MD161/19. We followed a two-step procedure to establish the correlation between NGHP-01-19B and MD161/20; first, the Toba-ash layer which is unambiguously identified on both the cores (NGHP-01-19B and MD161/20) was used as a marker event (**Fig. 6A**) for converting the depth-to-age assuming a uniform sedimentation rate. Next, we established peak-to-peak correlation of magnetic susceptibility records between NGHP-01-19B and MD161/20 and several tie points, as marked in the **Fig. 6A**, are established which are used as marker events to infer the age-depth model for the core MD161/20. The magnetic susceptibility record shows excellent peak to peak correlation between NGHP-01-19B and MD161/20 up to 80 ka suggesting similar fluctuation in magnetic mineral concentration associated with source provenance and depositional environment. The excellent correlation leads to good age control for the uppermost 20 mbsf (~ 80 ka). A similar fluctuation in magnetic susceptibility is also observed for the shallow sediments between the core MD161/19 and MD161/20 with minor age offset indicating that the age-depth relationship is reliable.

Further, the same age-depth relationship is applied to the wet-bulk density data measured onboard R/V *JOIDES Resolution* for core NGHP-01-19B (Collett et al., 2008) and onboard *D/V Marion Dufresne* for core MD161/20 (**Fig. 6B**). Some prominent peaks in wet-bulk density can be matched till 60 ka. Beyond 60 ka, the density data of core NGHP-01-19 show an abrupt drop that may not be reliable. Thus, the wet-bulk density data also support the age-depth relationship established from the magnetic susceptibility data.

6.3 Comparison between Holocene secular variation in KG and Mahanadi basins.

The PSV records from Mahanadi and KG basins during Holocene are compared (**Fig. 7**) with each other to understand the variability of Earth's magnetic field. Paleoinclination records from Mahanadi basin show pattern similar to that of KG basin (**Fig. 7A**) between 2.6 and 6.5 cal. ka BP despite significant variation in the sedimentation rate. A sharp drop in paleoinclination is observed around 4.2 cal. ka BP in both the basins. The paleoinclination (**Fig. 7B**) decreases from 4.2 to 2.8 cal. ka BP in both Mahanadi and KG basin. However, the PSV records for top 2.8 cal. ka BP could not be obtained in Mahanadi basin as the topmost sediment was soft with very high porosity/water content. Thus, the overall features in paleoinclination from KG basin are reproduced in Mahanadi basin although with a

lower resolution due to low sedimentation rate. Paleodeclination records of KG and Mahanadi basins show broad similarity, but we fail to establish one to one correlation.

6.4 Identification of known excursions (Mono lake, Laschamp and Norwegian-Greenland Sea) up to 80 ka

The paleoinclination, relative paleodeclination and normalized paleointensity values are plotted as a function of age for the core MD161/20 (**Fig. 8**). The reliable paleomagnetic records of Earth's magnetic field span from 80 ka to Recent in the Mahanadi basin. The older PSV records are not reliable and therefore not interpreted. The paleoinclination record of core MD161/20 exhibits four distinct intervals of negative paleoinclination. These zones of negative paleoinclination occur at ~9 mbsf (~18-20 ka), 13.5-15 mbsf (~42-49 ka), 16.3 mbsf (~54-57 ka) and 18-18.2 mbsf (~67-70 ka) (**Fig. 8A**). Numerous geomagnetic excursions are observed and identified globally such as Monolake (Denham and Cox, 1971; Liddicoat and Coe 1979; Negrini et al., 1984, 2000; Lund et al., 2001; Channell, 2006; Kissel et al., 2011), Laschamp (Bonhomet and Babkine 1967; Bonhomet and Zahringer 1969; Levi et al., 1990; Laj et al., 2000; Mazaud et al., 2002; Laj et al., 2006; Channell, 2006) and the split Norwegian-Greenland Sea events (Nowaczyk and Frederichs, 1994). The estimated age of these excursions are reported to be 27-36 ka BP (Monolake), ~41-45 ka (Laschamp), ~55 ka (Norwegian-Greenland Sea-I) and ~66 ka (Norwegian-Greenland Sea-II). Due to close association of the observed inclination anomalies in Mahanadi basin with the known excursions, the anomalies at 42-49 ka, 54-57 ka and 67-70 ka are correlated with Laschamp, Norwegian-Greenland Sea-I (NGS-I) and Norwegian-Greenland Sea-II (NGS-II) excursion events, respectively. We are unable to identify Monolake excursion in the paleomagnetic records from the Mahanadi basin. Further, the observed excursion event from 18-20 ka does not match with any known excursion event.

The relative paleodeclination shows a minor swing in declination towards negative values during NGS-I and NGS-II excursions. A slight positive swing in paleodeclination is observed for the Laschamp event (**Fig. 8B**). In general, a large swing in westerly declination is observed for Laschamp excursion (Levi and Karlin, 1989). Similarly, Thouveny et al., (2004) observed an eastward swing in declination during Laschamp excursion for the sedimentary sequences off Portuguese margin. A full reversal of 180° in declination was observed by Lund et al., (1998) during reversal excursion. In the present study, we do not observe large swing in declination for the excursion events. However, we cannot critically rely on paleodeclination data because it is a relative paleodeclination. Uncertainty in

paleodeclination may also arise during coring process due to twisting and turning (Ali et al., 1999) or it can be purely of geomagnetic origin due to local effects (Frank et al., 2002).

A minor drop in paleointensity is observed for the Laschamp, and a significant drop is observed for the NGS-I and NGS-II excursions in the Mahanadi basin (**Fig. 8C**). In general, the excursions are associated with a drop in paleointensity (Langereis et al., 1996, Roberts, 2008). Lund et al. (1998) also observed lower paleointensity during excursion but failed to establish evidence of higher than normal paleointensity after the excursion. The global character of the paleointensity covering the past 80 ka shows lows in paleointensity at ~20, ~40 and ~60-70 ka (Tric et al., 1992, Meynadier et al., 1992). we also observe lows in paleointensity at these time intervals although low at 20 ka is not observed clearly. We should be careful in interpreting the relative paleointensity record as it is difficult to remove the effect of magnetic grain size variations from the paleointensity estimates (Schwartz et al., 1996).

In paleomagnetism, it is not possible to interpret significant swing in inclination or declination records directly to the geomagnetic excursion. This swing in inclination or declination may represent local effect or diagenetic alterations (Van Hoof et al., 1993). Therefore, it is essential to verify that the anomalies are not associated with any changes in magnetic mineralogy, concentration or grain size (Verosub, 1975) or depositional environment. In the present study, detailed rock magnetic measurements are studied near the observed anomalies to observe any abrupt change in magnetic mineralogy, concentration or grain size. The rock magnetic parameters of MD161/20 (χ_{LF}, χ_{ARM} and SIRM) do not show any abrupt change in the zones of negative paleoinclination (**Fig. 4A**). The magnetic extracts from different depths also do not show any abrupt changes in magnetic mineralogy, and the dominant magnetic minerals are titanomagnetite/titanohematite with varying Ti-content (**Fig. 5**).

Next, we analyze the changes in depositional environed during the past 80 ka in the Mahanadi basin. The major clay minerals in the Mahanadi basin are Ilite (23-64 %) and Smectite (9.6-53.6 %) (Mazumdar et al., 2015). Based on the major and trace element analysis, the source rock composition of Mahanadi sediments is closed to the mixture of Archean granite and TTG (Tonalite-Trondhjemite Gneiss) derived product. We do not have the lithological and sedimentological data for the core MD161/20. Therefore, we rely on the lithostratigraphy (Collett et al., 2008) and sedimentological data (Phillips et al., 2014) of the core NGHP-01-19B to understand the depositional environment in

Mahanadi basin (**Fig. 9**). The inclination anomaly around 20 ka lies within the Nanofossil bearing clay, Laschamp anomaly lies within Nanofossil rich foram bearing clay, NGS-I lies within Nanofossil rich pyrite-bearing clay, and NGS-II lies within the clay. All the major inclination anomalies lie within the clay, and therefore lithology variation may not be related to the observed inclination anomalies. Phillips et al. (2014) reported the sedimentological data for the core NGHP-01-19B in the Mahanadi basin. The dominant grain size of carbonate-free, predominantly lithogenic sediment is silt (56-86%) followed by clay fraction (11-37%) and sand-sized content (0-6%). Negligible variation is observed for the lithogenic grain size from 80 ka to Recent. Mass accumulation rate (MAR) of total organic content (TOC) varies from 0.03 to 0.44 g/cm3/kyr. The MAR of TOC is low (0.03g/cm3/kyr) between 29-20 ka and high (0.44 g/cm3/kyr) at 10 ka. A slight increase in MAR of TOC is observed between 80 and 29 ka due to high TOC content. In addition, the ratio of biogenic MAR to lithogenic MAR varies between 0.04 and 0.36 and closely matches the pattern in $CaCO_3$ content. It is maximum around 20 ka and increases slightly from 70 ka to 30 ka. We do not find a significant anomaly in the sedimentological data corresponding to the Laschamp, NGS-I and II excursion events. However, low MAR of TOC and high ratio of biogenic MAR to lithogenic MAR is observed near 20 ka anomaly during the Last Glacial Maximum (LGM). Phillips et al., (2014) attributed these changes to the decrease in monsoonal precipitation during glacial period which not only increases the $CaCO_3$ production but also reduces the chemical weathering leading to higher susceptibility with increased Ti-content. Colin et al. (1998) and Sangode et al. (2001) also reported increase in susceptibility and magnetic grain size during the LGM. Therefore, we attribute the inclination anomaly around 20 ka to local effect due to the change in depositional environment.

6.5 Virtual Geomagnetic Pole (VGP) estimation of Laschamp and NGS-I and II excursions

The virtual geomagnetic poles (VGP) are calculated from the observed paleo-inclination and declination, and its path associated with Laschamp and Norwegian-Greenland Sea excursion is shown in **Fig. 10.** Laschamp excursion, one of the widely studied and well-established excursions in Brunhes chron, shows well-defined VGP trace showing large departure of geomagnetic field vector from its normal position and reaching high southerly latitudes in a clockwise loop, and thereafter it swings back to northerly latitudes. The VGP loop for Laschamp agrees with the clockwise loop as observed globally (Laj et al., 2006; Roberts, 2008, Lund and Schwartz, 2005). In contrast, the NGS-I and NGS-II VGP trace are not well established, but it also shows a large swing towards the high southern latitude and oscillations in the tropics.

7. Conclusions

A high-resolution paleomagnetic investigation performed on the core MD161/20 from Mahanadi basin yielded a reliable paleoinclination record for past 80 ka. The record shows the presence of the three known geomagnetic excursion events during Brunhes chron: Laschamp (~42-49 ka), Norwegian-Greenland Sea-I (~54-57 ka) and Norwegian-Greenland Sea-II (~67-70 ka) in the Bay of Bengal. The VGP path traced by Laschamp excursion shows a clockwise loop as reported globally. The excursions seem to occur in the periods of relatively low paleointensity. No reliable paleomagnetic results are obtained for records older than 80 ka, and warrants further investigations in the Bay of Bengal.

Acknowledgements

The authors thank the Director, CSIR-NIO for his support and permission to publish the paper. We also thank the Directors of NIOT and NCAOR, and the Secretary, Ministry of Earth Sciences for providing financial support for sediment coring on board RV Marion Dufresne. The crew from NIO, NIOT and NGRI and students from Goa University are also acknowledged for their support during the acquisition of cores. Daryl Vaz is acknowledged for preparing final figures. Mr. Kanala, K. K. is acknowledged for some magnetic measurements at NIO. VNJCT fellowship to Ms. Asha Usapkar is sincerely acknowledged. We thank the anonymous reviewers and associate editor for constructive comments/suggestions which has improved the quality of the manuscript. This is CSIR contribution no…..

References

Acharyya, S.K., Basu, P.K., 1993. Toba ash on the Indian subcontinent and its implications for correlation of Late Pleistocene Alluvium. Quaternary Resources 40, 10-19.

Ali. M., Oda, H., Hayashida, A., Takemura, K., Torri, M., 1999. Holocene paleomagnetic secular variation at Lake Biwa, central Japan. Geophys. J. Int., 218-228.

Bailey, M.E., Dunlop, D.J., 1983. Alternating field characteristics of pseudo-single-domain (2-14 μm) and multidomain magnetite. Earth and Planetary Science Letters 63, 335-352.

Bloemendal, J., Lamb, B., King, J., 1988. Palaeoenvironmental implications of rock magnetic properties of late Quaternary sediment cores from the eastern equatorial Atlantic. Paleooceanography 3, 61-87.

Bloemendal, J., King, J.W., Hall, F.R., Doh, S.-J., 1992. Rock magnetism of Late Neogene and Pleistocene deep-sea sediments: relationship to sediment source, diagenetic processes, and sediment lithology. Journal of Geophysics Resources 97, 4361-4375.

Bonhommet, N., Babkine, J., 1967. Sur la presence d'aimentation inverse dans la Chaine des Puys. C.R. Hebs. Seances Acad. Sci. Ser.B. 264, 92-94.

Bonhommet, N., Zahringer, J., 1969. Paleomagnetism and potassium argon determinations of the Laschamp geomagnetic polarity event. Earth and Planetary Science Letters 6, 43-46.

Chakrapani, G.J., Subramanian, V., 1990. Preliminary studies on the geochemistry of the Mahanadi river basin, India. Chemical Geology 81, 241-253.

Chakrapani, G.J., Subramanian, V., 1993. Heavy metals distribution and fractionation in sediments of the Mahanadi River basin, India. Environmental Geology 22, 80-87.

Chakrapani, G.J., Subramanian, V., 1993. Rates of erosion and sedimentation in the Mahanadi river basin, India. Journal of Hydrology 149, 39-48.

Champion, D.E., Lanphere, M.A., Kuntz, M.A., 1988. Evidence for a new geomagnetic reversal from lava flows in Idaho: Discussion of short polarity reversals in the Brunhes and late Matuyama polarity chrons, Journal of Geophys. Res. 93, 11667-11680.

Channell, J.E.T., 2006. Late Brunhes polarity excursions (Monolake, Laschamp, Iceland basin and Pringle Falls) recorded at ODP site 919 (Irminger Basin). Earth and Planetary Science Letters 244, 378-393.

Channell, J.E.T., Xuan, C., 2009. Self-reversal and apparent magnetic excursions in Arctic sediments. Earth and Planetary Science Letters 284, 124-131.

Colin, C., Kissel, C., Blamart, D., Turpin, L., 1998. Magnetic properties of sediments in the Bay of Bengal and the Andaman Sea: impact of rapid North Atlantic Ocean climatic events on the strength of the Indian monsoon. Earth and Planetary Science Letters, 160(3), 623-635.

Collett, T.S., Riedel, M., Cochran, J.R., Boswell, R., Presley, J., Kumar, P., Sathe, A., Sethi, A., Lall, M., Sibal, V., NGHP Expedition 01 Scientists, 2008. National Gas Hydrate Program Expedition 01 Initial Reports. Directorate General of Hydrocarbons, New Delhi.

Dekkers, M.J., Langereis, C.G., Vriend, S.P., van Santvoort, P.J.M., de Lange, G.J., 1994. Fuzzy c-means cluster analysis of early diagenetic effects on natural remanent magnetization acquisition in a 1.1 Myr piston core from the central Mediterranean. Physics of Earth and Planetary Interiors 85, 155-171.

Denham, C.R., Cox, A., 1971. Evidence that the Laschamps polarity event did not occur 13300-30400 years ago. Earth Planetary Science Letters 13, 181-190.

Dunlop, D.J., 1973. Superparamagnetic and single domain threshold sizes in magnetite. Journal of Geophysics Resources 78, 1780-1793.

Dunlop, D.J., Xu, S., 1994. Theory of partial remanent magnetization in multidomain grains. 1. Repeated identical barriers to wall motion (single microcoercivity) 1994. Journal of Geophysical Research 99, 9005-9023.

Dunlop, D.J., Özdemir, Ö., 1997. Rock magnetism: fundamentals and frontiers. New York: Cambridge University Press.

Frank, U., Nowaczyk, N.R., Negendank, J.F.W., Melles, M., 2002. A paleomagnetic record from Lake Lama, northern Central Siberia. Physics of Earth and Planetary Interiors 133, 3-20.

Gubbins, D., 1991. Convection in the Earth's core and mantle-harold Jeffreys Lecture. Quaternary Journal of the Royal Astronomical Society 32, 69-84.

Hanna, R.L., Verosub, K.L., 1989. A review of lacustrine paleomagnetic records from western North America: 0-40 000 years BP. Physics of the Earth and Planetary Interiors 56, 76-95.

Heider, F., Dunlop, D.J., 1987. Two type of chemical remanent magnetization during oxidation of magnetite. Physics of Earth and Planetary Interiors 46, 24-45.

Herrero-Bervera, E., Helssley, C.E., Hammond, S.R., Chitwood, L.A., 1989. A possible lacustrine paleomagnetic record of the Blake episode from Pringle Falls, Oregon, U.S.A. Physics of Earth and Planetary Interiors 56, 112-113.

Herrero-Bervera, E., Helsley, C.E., Sarma-Wojcicki, A.M., Lajoie, K.R., Meyer, C.E., McWilliams, M.O., Negrini, R.M., Turrin, B.D., Donnelly-Nplan, J.M., Liddicoat, J.C., 1994. Age and correlation of a paleomagnetic episode in the western United States by ^{40} Ar/^{39} Ar dating and tephrochronology: the Jamaica, blake, or a new polarity episode? Journal of Geophys. Res. 99, 24, 091-24, 103.

Heslop, D., 2009. On the statistical analysis of the rock magnetic S-ratio. Geophysics Journal International 178, 159-161.

Kissel, C., Guillou, H., Laj, C., Carracedo, J.C., Nomade, S., Perez-Torrado, F., Wandres, C., 2011. The Mono Lake excursion recorded in phonolitic lavas from Tenerife (Canary Islands): Paleomagnetic analyses and coupled K/Ar and Ar/Ar dating. Phys. Earth Planet. Inter. 187, 232–244. doi:10.1016/j.pepi.2011.04.014.

Kirschvink, J.L., 1980. The least-squares line and plane and the analysis of paleomagnetic data. Geophysical Journal of the Royal Astronomical Society 62, 699-718.

Laj, C., Kissel, C., Mazaud, A., Channell, J.E.T., Beer, J., 2000. North Atlantic paleointensity stack since 75 ka (NAPIS-75) and the duration of the Laschamp event. Phil. Trans.R. Soc. Series A, 358, 1009-1025.

Laj, C., on board party, 2006. MD 155-Macro Polo 2 IMAGES XIV cruise report, des rapports de campagnes à la mer. IPEV.

Langereis, C.G., Dekkers, M.J., de Lange, G.J., Paterne, M., van Santvoort, P.J.M., 1997. Magnetostratigraphy and astronomical calibration of the last 1.1 Myr from an eastern Mediterranean piston core and dating of short events in the Brunhes. Geophysics Journal International 129, 75-94.

Levi, S., Gudmunsson, H., Duncan, R.A., Kristjansson, L., Gillot, P.V., Jacobsson, S.P., 1990. Late Pleistocene geomagnetic excursion in Icelandic lavas: confirmation of the Laschamp excursion. Earth Planetary Science Letters 96, 443-457.

Levi, S., Karlin, R., 1989. A sixty thousand year paleomagnetic record from Gulf of California sediments: Secular variation, late Quaternary excursions and geomagnetic implications. Earth and Planetary Science Letters 92, 219-233.

Liddicoat, J.C, Coe, R.S., 1979. Monolake Geomagnetic excursion. Journal of Geophysical Research: Solid Earth 84, 261-271.

Liu, Q., Roberts, A.P., Torrent, J., Horng, C.-S., Larrasoaña, J.C., 2007. What do the HIRM and S-ratio really measure in environmental magnetism? Geochemistry Geophysics Geosystems 8. Q09011.

Lund, S.P., Williams, T., Acton, G.D., Clement, B., Okada, M., 2001. Brunhes chron magnetic field excursions recovered from Leg 172 sediments 2001. In Keigwin , L.D., Rio, D., Acton, G.D., Arnold, E. (Eds.), Proceedings of the ocean drilling program, scientific results 172, 1-18.

Lund, S.P., Schwartz, M., 2005. Deep-sea sediment records of the Laschamp geomagnetic field excursion (~41, 000 calendar years before present). Journal of Geophysical Research 110, B04101, doi: 10.1029/2003JB002943.

Lund, S.P., Acton, G., Clement, B., Hastedt, M., Okada, M., Williams, T., 1998. Geomagnetic field excursions occurred often during the last million years. EOS Transactions of the American Geophysical Union 78, S178-S179.

Maher, B.A., 1988. Magnetic properties of some synthetic sub-micron magnetites. Geophysics Journal International 94, 83-96.

Maher, B.A., Taylor, R.M., 1988. Formation of ultrafine-grained magnetite in soils. Nature 336, 368-370.

Mazaud, A.S., Ezat, M.A., Pichon, U., Duprat, J.J., Laj, C., Kissel, C., Beaufort, L., Michel, E., Turon, J.L., 2002. Geomagnetic-assisted stratigraphy and sea surface temperature changes in core MD94-103 (Southern Indian Ocean): possible implications from North-South climatic relationships around H4. Earth and Planetary Science 201.

Mazumdar, A., Kocherla, M., Carvalho, M.A., Peketi, A., Joshi, R.K., Mahalaxmi, P., Joao, H.M., Jisha, R., 2015. Geochemical characterization of the Krishna–Godavari and Mahanadi offshore basin (Bay of Bengal) sediments: a comparative study of provenance. Marine and Petroleum Geology 60, 18-33.

Mazumdar, A., Peketi, A., Joao, H.M., Dewangan, P., Ramprasad, T., 2014. Pore-water chemistry of sediment cores off Mahanadi basin, Bay of Bengal: Possible link to deep seated methane hydrate deposit. Marine and Petroleum Geology 49, 162-175.

Meynadier, L., Valet, J-P., Weeks, R., Shackelton, N.J., Hagee, V.L., 1992. Relative geomagnetic intensity of the field during the last 140 ka. Earth and Planetary Science Letters 114, 39-57.

Nowaczyk, N.R., Baumann, M., 1992. Combined high-resolution magnetostratigraphy and nannofossil biostratigraphy for late Quaternary Arctic Ocean sediments. Deep Sea Res., Part A, 39, 567-601.

Nowaczyk, N.R., Frederichs T.W.,1999. Geomagnetic events and relative palaeointensity variations during the past 300 ka as recorded in Kolbeinsey Ridge sediments, Iceland Sea: Indication for a strongly variable geomagnetic field. Int. J. Earth Sci., 88, 116-131.

Negrini, R.M., Davis, J.O., Verosub, K.L., 1984. Mono Lake geomagnetic excursion found at Summer Lake, Oregon. Geology 12, 643-646.

Negrini, R.M., Verosub, K.L., Davis, J.O., 1987. Long-term nongeocentric axial dipole directions and a geomagnetic excursion from the middle Pleistocene sediments of the Humboldt River canyon, Pershing Country, Nevada. Journal of Geophys. Res. 92(10), 610-617.

Negrini, R.M., Erbes, D.B., Faber, K., Herrera, A.M., Roberts, A.P., Cochen, A.S., Wigand, P.E., Feanklin, F.F Jr., 2000. A paleoclimate record for the past 250, 0000 years from summer Lake, Oregon, USA: I. Chronology and magnetic proxies for lake level. Journal of Paleolimnology 24, 125-149.

Ninkovitch, D., 1979. Distribution, age and chemical composition of tephra layers in the deep-sea sediments off western Indonesia. Journal of Volcanol. Geotherm. Res. 5, 67-86.

Nowaczyk, N.R., Frederichs, T.W., Eisenhauer, A., Gard, G., 1994. Magnetostratigraphic data from late Quaternary sediments from the Yermak Plateau, Arctic Ocean: evidence for four geomagnetic polarity events within the last 170 ka of the Brunhes Chron 117, 453-471.

Oldfield, F., Yu, L., 1994. The influence of particle size variations on the magnetic properties of sediments from the north-eastern Irish Sea. Sedimentology 41, 1093-1108.

O'Regan, M., King, J., Backman, J., Jakobsson, M., Palike, H., Moran, K., Heil, C., Sakamoto, T., Cronin, T.M., Jordan, R.W., 2008. Constraints on the Pleistocene chronology of sediments from the Lomonosov Ridge. Paleooceanography 23, PA 1s19, http://dx.doi.org/10.1029/2007PA001551.

Phillips, S.C., Johnson, J.E., Giosan, L., Rose, K., 2014. Monsoon-influenced variation in productivity and lithogenic sediment flux since 110 ka in the offshore Mahanadi basin, northern Bay of Bengal. Marine and Petroleum Geology 58, 502-525.

Rao, D.G., Krishna, K.S., 1997. Crustal evolution and sedimentation history of the Bay of Bengal since the Cretaceous. Journal of Geophysical Research 102 (B8), 17,747-17,768.

Roberts, A.P., 2008. Geomagnetic excursions: Knowns and unknowns. Geophysical Research Letters 35, L17307, doi: 10.1029/2008GL034719.

Roperch, P., Bonhommet, N., Levi, S., 1988. Paleointensity of the earth's magnetic field during the Laschamp excursion and it's geomagnetic implications. Earth and Planetary Science Letters 88, 209-219.

Sastri, V.V., Venkatachala, B.S., Narayanan, V., 1981. The evolution of the east coast of India. Palaeogeography, Paleoclimatology, Paleoecology 36, 23-54.

Schwartz, M., Lund, S.P., Johnson, T.C., 1996. Environmental factors as complicating influences in the recovery of quantitative geomagnetic-field paleointensity estimates from sediments. Geophysical research letters, 23(19), pp.2693-2696.

Singh, I., 2008. Mahanadi basin (Mahanadi-NEC Basin) Oil and Gas Fields of India. Indian Petroleum publishers, Dehradun, India, 325-346.

Smith, J.D., Foster, J.H., 1969. Geomagnetic reversal in the Brunhes normal polarity epoch. Science 163, 565-567.

St-Onge G., Stoner, J.S., Hillaire-Marcel, C., 2003. Holocene paleomagnetic records from the St. Lawrence Estuary, eastern Canada: Centennial to millennial-scale geomagnetic modulation of cosmogenic isotopes. Earth and Planetary Science Letters 209, 113-130.

Subrahmanyam, V., Subrahmanyam, A.S., Murty, G.P.S., Murthy, K.S.R., 2008. Morphology and tectonics of Mahanadi basin, northeastern continental margin of India from geophysical studies. Marine Geology 253, 63-72.

Subramanian, V., 1980. Mineralogical input of suspended matter by Indian rivers into the adjacent areas of the Indian Ocean. Marine Geology 36, 29-34.

Tauxe, L., 1993. Sedimentary records of relative paleointensity of the geomagnetic field: theory and practice. Reviews of Geophysics 31(3), 319-354.

Thompson, R., Oldfield, F., 1986. Environmental magnetism. Allen and Unwin, 227pp.

Thouveny, N., Carcaillet, J., Moreno, E., et al., 2004. Geomagnetic moment variation and paleomagnetic excursions since ka BP: A stacked record from sedimentary sequences of the Portuguese margin. Earth and Planetary Science Letters 219,

Tric, E., Laj, C., Valet, J.-P., Tucholka, P., Paterne, M., Guichard, F., 1991. The Blake geomagnetic event: transition geometry, dynamical characteristics and geomagnetic significance, Earth and Planetary Science Letters 102, 1-13.

Tric,E., Valet,J.P., Tucholka, P., Parterne, M., Labeyrie, L., Guichard, F., Tauxe, L., Fontune, M., 1992. Paleointensity of the geomagnetic field during the last gighty thousand years. Journal of Geophys. Res. 97, 9337-9351.

Tucholka, P., Fontugne, M., Guichard, F., Paterne, M., 1987. The Blake magnetic polarity episode in cores from the Mediterranean Sea. Earth Planetary Science Letters 86, 320-326.

Van Hoof, A.A.M., Van Os, B.J.H., Rademakers, J.G., Langereis, C.G., de Lange, G.J., 1993. A paleomagnetic and geochemical record of the upper Cochiti reversal and two subsequent precessional cycles from Southern Sicily. Earth and Planetary Science Letters 117, 235-250.

Verosub, K.L., 1975. Paleomagnetic excursions as magnetostratigraphic horizons: a cautionary note. Science 190, 48-50.

Verosub, K.L., Banerjee, S.K., 1977. Geomagnetic excursions and their paleomagnetic record. Journal of Geophys. Res. 15, 145-155.

Verosub, K.L., 1982. Geomagnetic excursions: a critical assessment of the evidence as recorded in sediments of the Brunhes Epoch. Philosophical Transactions of the Royal Society of London A: Mathematical, Physical and Engineering Sciences 306, 161-168.

Walden, J., Oldfield, F., Smith, J.P., (Eds), 1999. Environmental Magnetism: A Practical Guide. Technical Guide, No. 6, Quaternary Research Association, London.

Zhu, R., Gu, Z., Huang, B., Jin, Z., Wei, X., Li, C., 1994. Geomagnetic secular variations and climate changes since 15, 000 a BP., Beijing region. Science in China Series B, Chemistry, life Sciences & earth sciences 37, 984-990.

Zijderveld, J.D.A., 1967. A.C. demagnetisation of rock: analysis of results. In: Collinson, D.W., Creer, K.M., Runcorn, S.K. (Eds.), Methods in Paleomagnetism. Elsevier, Amsterdam, the Netherlands, pp. 254-286.

Figures captions

Fig. 1. Location map of the study area in Mahanadi basin, Bay of Bengal. Black star represents location of the study core. (Location map modified after Mazumdar et al., 2014). The location of the core NGHP-01-19B and MD161/19 is shown for reference.

Fig. 2 A, B. Orthogonal projection of Zijderveld vector end plot diagrams. Circles and squares represent projection on the vertical and horizontal plane.

Fig. 3. A) Paleoinclination, B) paleodeclination, C) paleointensity and D) maximum angle of deviation (MAD) of MD161/20 (MD 20) with respect to depth.

Fig. 4A. Downcore variation in χ_{LF}, χ_{ARM} and SIRM of MD161/20 (MD 20) with respect to depth.

Fig. 4B. Downcore variation in χ_{FD} (%), χ_{ARM}/SIRM and SIRM/χ_{LF} of MD161/20 with respect to depth.

Fig. 4C. Downcore variation in Soft-IRM, Hard-IRM and S-ratio of MD161/20 with respect to depth.

Fig. 5. The SEM-EDS analysis of magnetic extracts from different depths.

Fig. 6. A) Stratigraphic correlation between the core NGHP-01-19B and the core MD161/20 using magnetic susceptibility. B) The correlation is shown between the two cores using density data.

Fig. 7. Comparison of A) paleoinclination and B) paleodeclination records from KG and Mahanadi basin.

Fig. 8. A) Paleoinclination, B) paleodeclination and C) paleointensity of MD161/20 (MD 20) with respect to age.

Fig. 9. Lithostratigraphy of the core NGHP-01-19B (modified after Collett et al., 2008).

Fig.10. Virtual geomagnetic pole (VGP) path traced by Laschamp and Norwegian-Greenland Sea excursions in Mahanadi basin.

Table captions

Table 1. Downcore variation of inclination, declination and paleointensity of MD161/20 at 50 cm resolution for top 20 m.

Table 2. Downcore variation in rock magnetic parameters for the core MD161/20 for the top 20 m.

Figure - 1

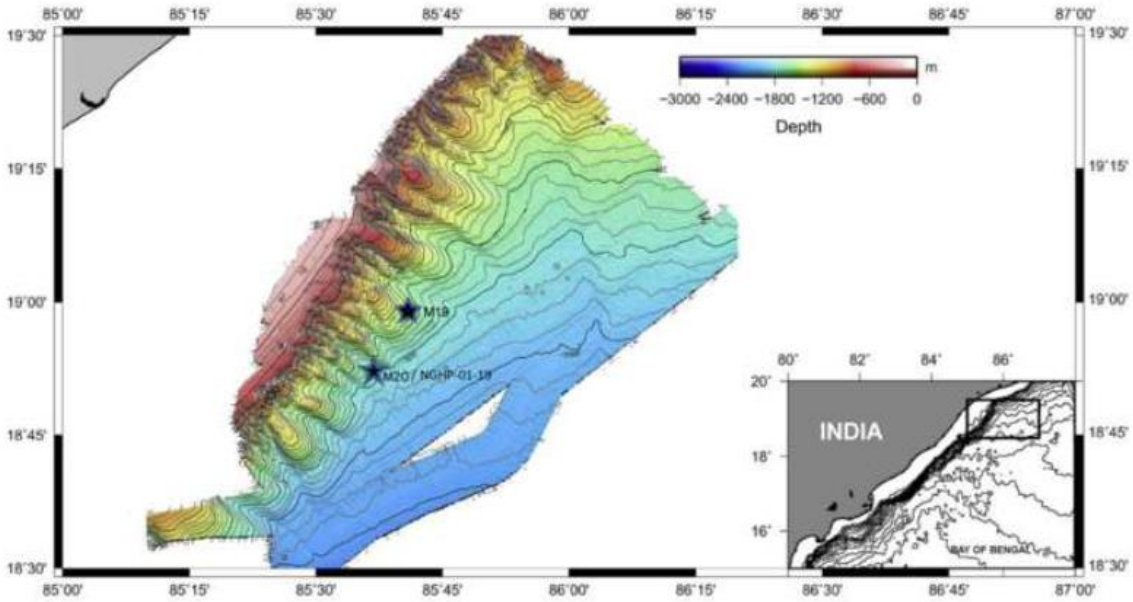
85°00'
85°15'
85°30'
85°45'
86°00'
86°15'
86°30'
86°45'
87°00'
19°30'
19°15'
19°00'
18°45'
18°30'
m
−3000 −2400 −1800 −1200 −600 0
Depth
M19
M20 / NGHP-01-18
80°
82°
84°
86°
20°
18°
16°
INDIA
BAY OF BENGAL

Figure - 2A

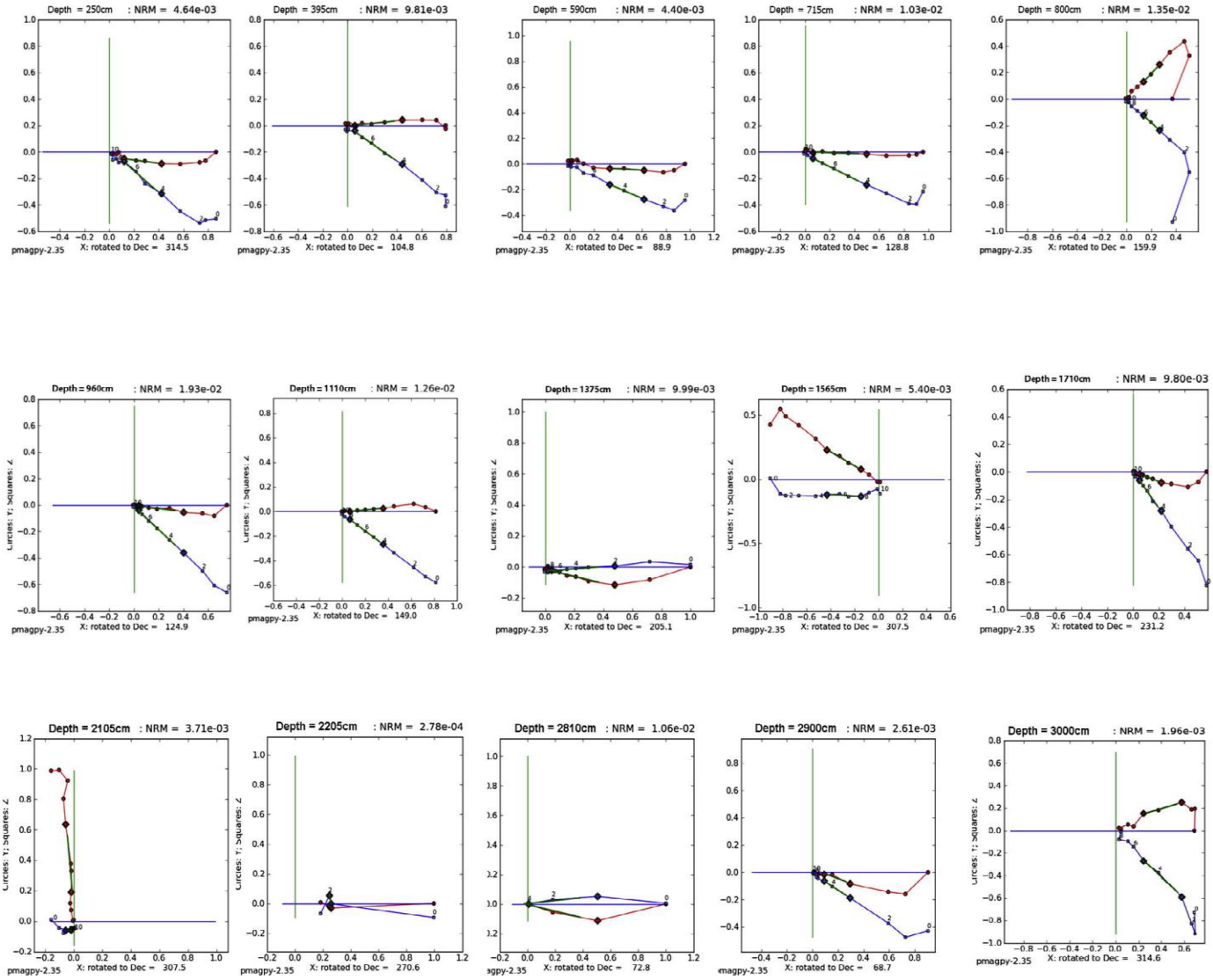
Depth = 250cm : NRM = 4.64e-03
X: rotated to Dec = 314.5
Depth = 395cm : NRM = 9.81e-03
X: rotated to Dec = 104.8
Depth = 590cm : NRM = 4.40e-03
X: rotated to Dec = 88.9
Depth = 715cm : NRM = 1.03e-02
X: rotated to Dec = 128.8
Depth = 800cm : NRM = 1.35e-02
X: rotated to Dec = 159.9
Depth = 960cm : NRM = 1.93e-02
X: rotated to Dec = 124.9
Depth = 1110cm : NRM = 1.26e-02
X: rotated to Dec = 149.0
Depth = 1375cm : NRM = 9.99e-03
X: rotated to Dec = 205.1
Depth = 1565cm : NRM = 5.40e-03
X: rotated to Dec = 307.5
Depth = 1710cm : NRM = 9.80e-03
X: rotated to Dec = 231.2
Depth = 2105cm : NRM = 3.71e-03
X: rotated to Dec = 307.5
Depth = 2205cm : NRM = 2.78e-04
X: rotated to Dec = 270.6
Depth = 2810cm : NRM = 1.06e-02
X: rotated to Dec = 72.8
Depth = 2900cm : NRM = 2.61e-03
X: rotated to Dec = 68.7
Depth = 3000cm : NRM = 1.96e-03
X: rotated to Dec = 314.6

Figure - 2B

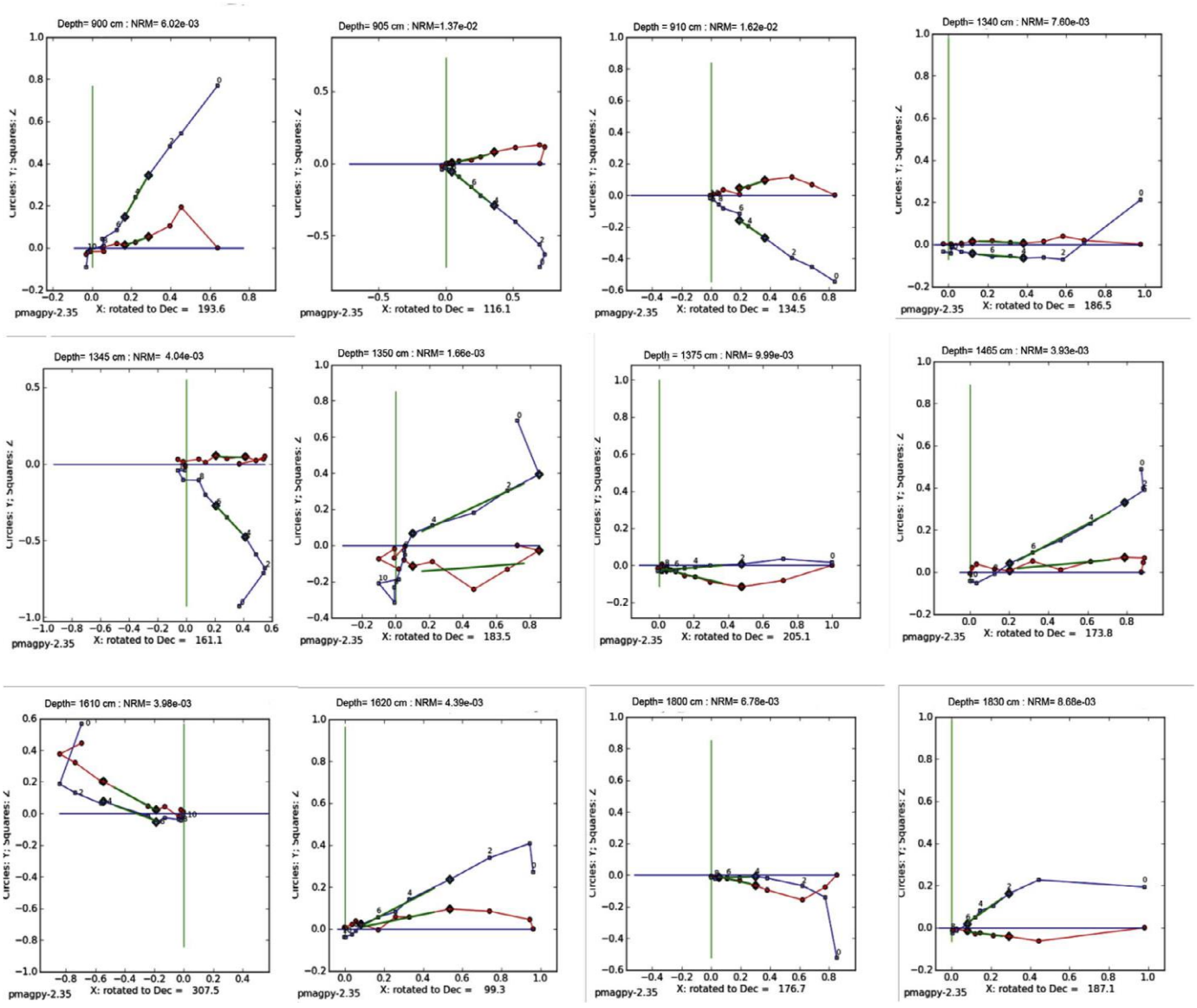
Depth= 900 cm : NRM= 6.02e-03
Depth= 905 cm : NRM=1.37e-02
Depth = 910 cm : NRM= 1.62e-02
Depth= 1340 cm : NRM= 7.60e-03
Depth= 1345 cm : NRM= 4.04e-03
Depth= 1350 cm : NRM= 1.66e-03
Depth = 1375 cm : NRM= 9.99e-03
Depth= 1465 cm : NRM= 3.93e-03
Depth= 1610 cm : NRM= 3.98e-03
Depth= 1620 cm : NRM= 4.39e-03
Depth= 1800 cm : NRM= 6.78e-03
Depth= 1830 cm : NRM= 8.68e-03
Circles: Y; Squares: Z
pmagpy-2.35
X: rotated to Dec = 193.6
X: rotated to Dec = 116.1
X: rotated to Dec = 134.5
X: rotated to Dec = 186.5
X: rotated to Dec = 161.1
X: rotated to Dec = 183.5
X: rotated to Dec = 205.1
X: rotated to Dec = 173.8
X: rotated to Dec = 307.5
X: rotated to Dec = 99.3
X: rotated to Dec = 176.7
X: rotated to Dec = 187.1

Figure – 3

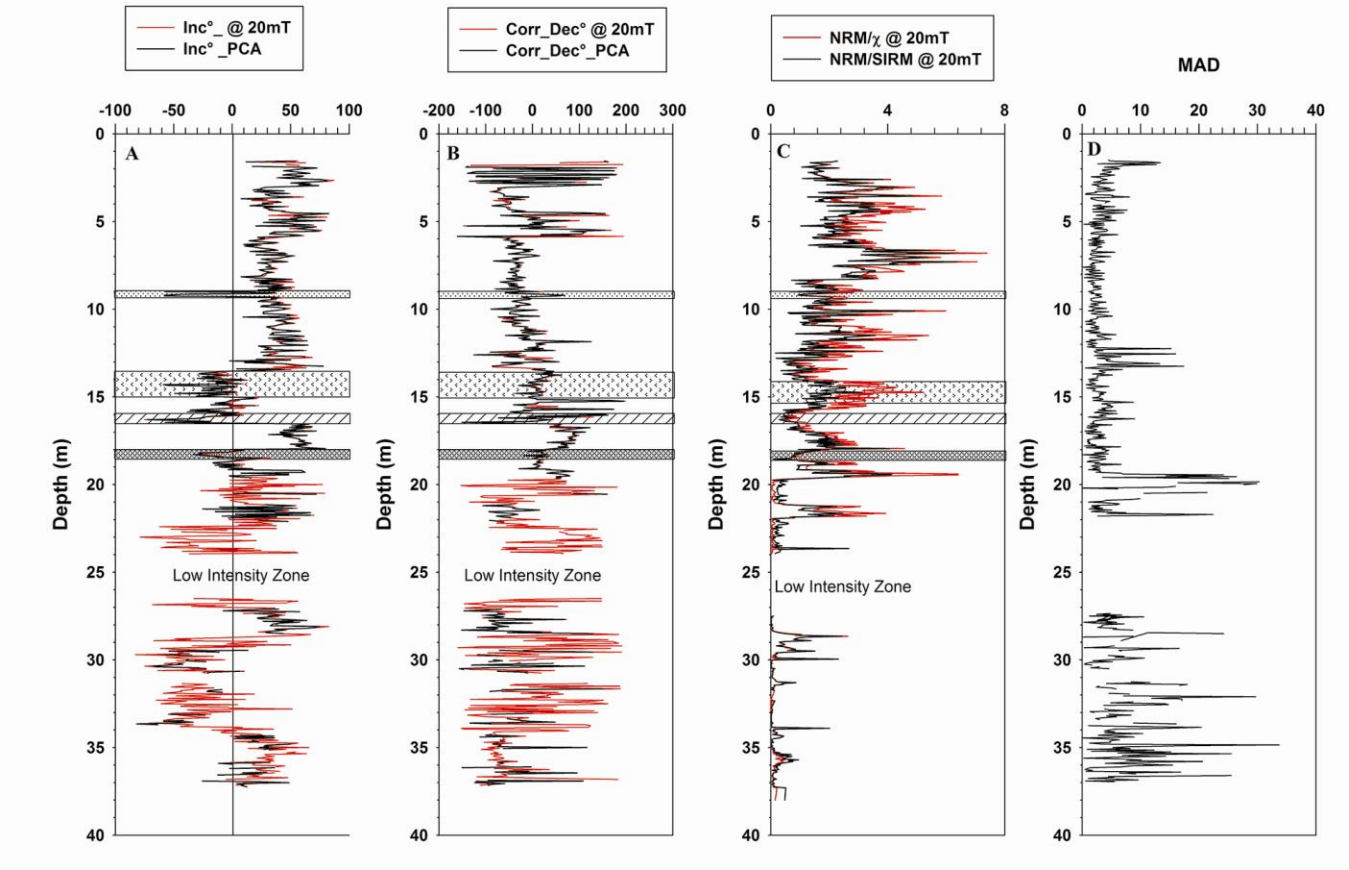
Inc°_ @ 20mT
Inc° _PCA
Corr_Dec° @ 20mT
Corr_Dec°_PCA
NRM/χ @ 20mT
NRM/SIRM @ 20mT
MAD
A
B
C
D
Depth (m)
Low Intensity Zone
Low Intensity Zone
Low Intensity Zone

Figure - 4A

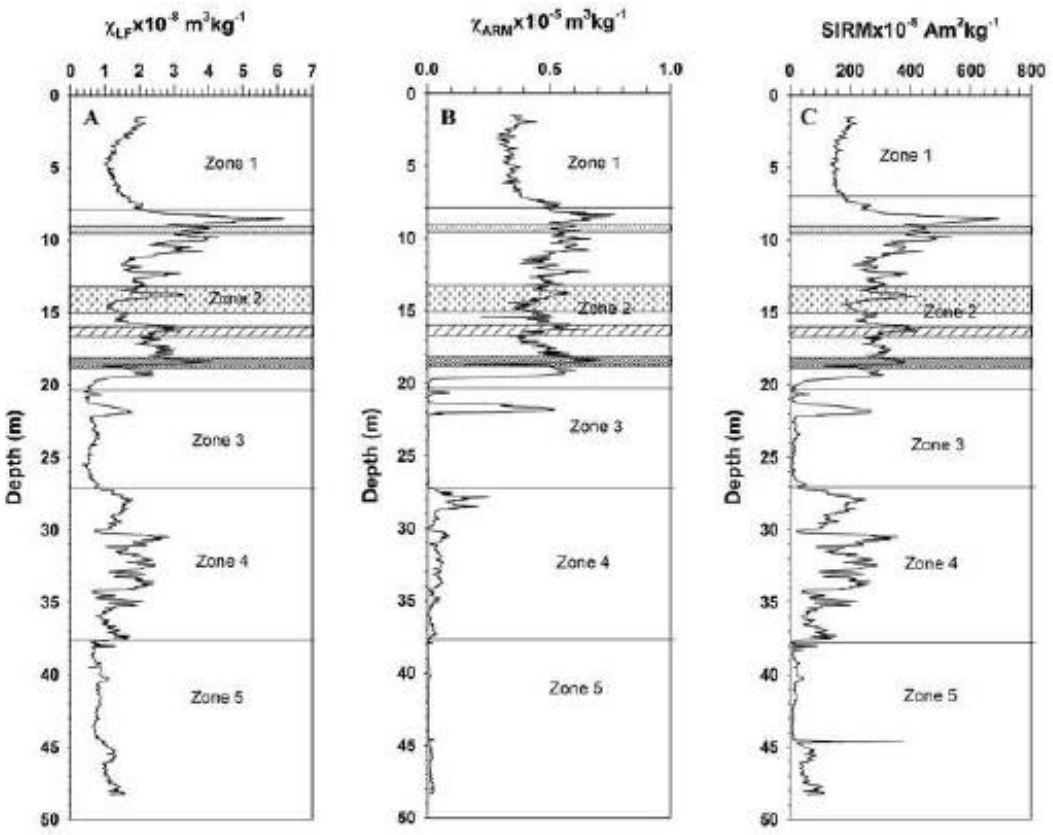
χ_{LF}×10^{-8} m^{3}kg^{-1}
χ_{ARM}×10^{-5} m^{3}kg^{-1}
SIRMx10^{-5} Am^{2}kg^{-1}
Depth (m)
A
B
C
Zone 1
Zone 2
Zone 3
Zone 4
Zone 5

Figure - 4B

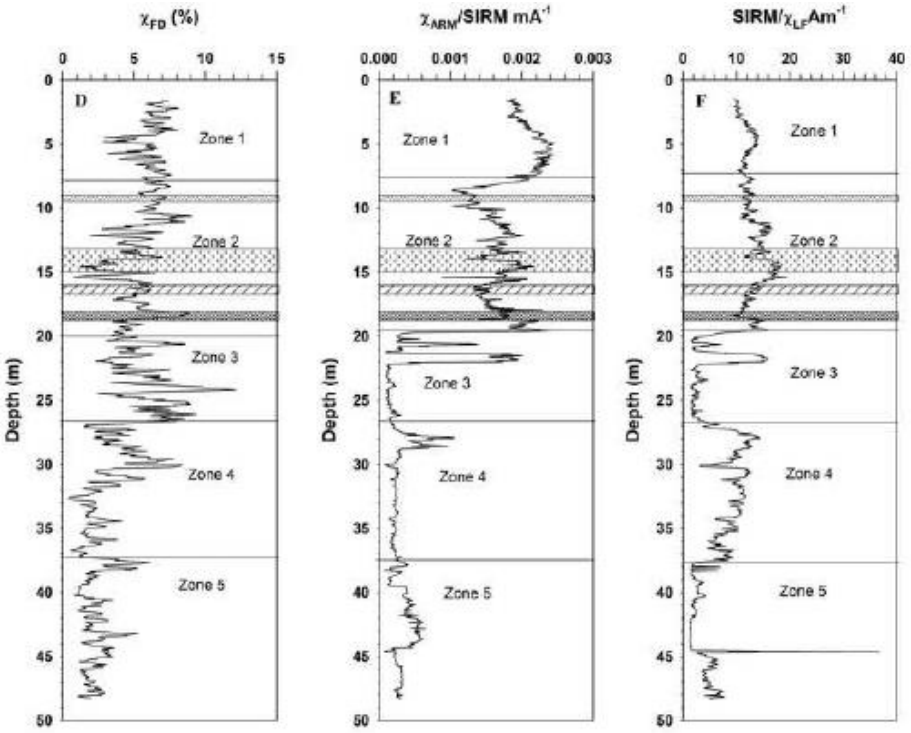

Figure - 4C

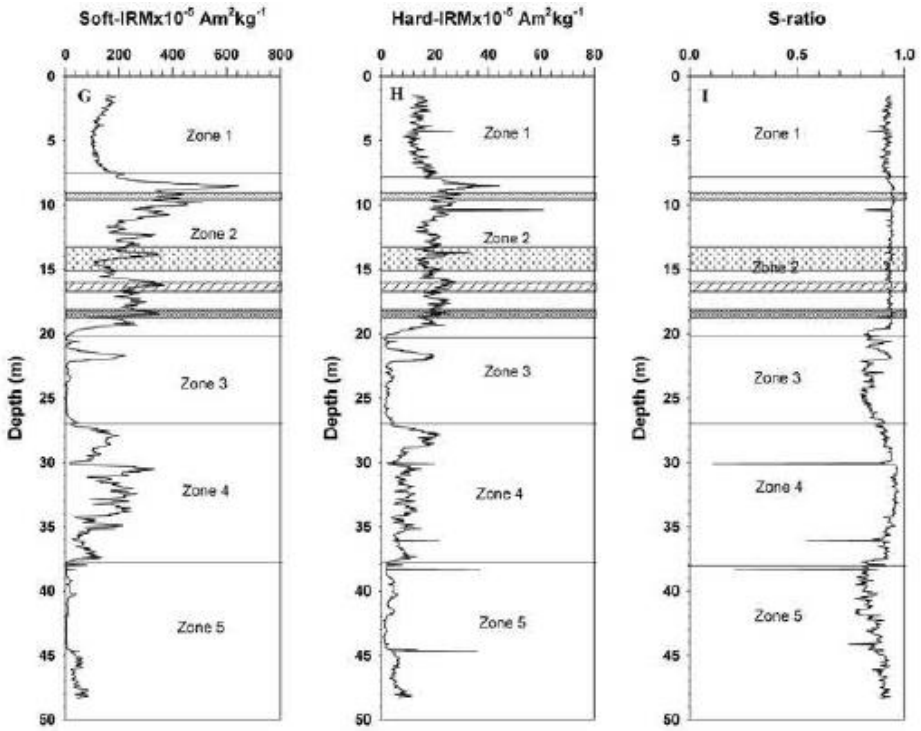
Soft-IRMx10⁻⁵ Am²kg⁻¹
Hard-IRMx10⁻⁵ Am²kg⁻¹
S-ratio
Depth (m)
G
H
I
Zone 1
Zone 2
Zone 3
Zone 4
Zone 5

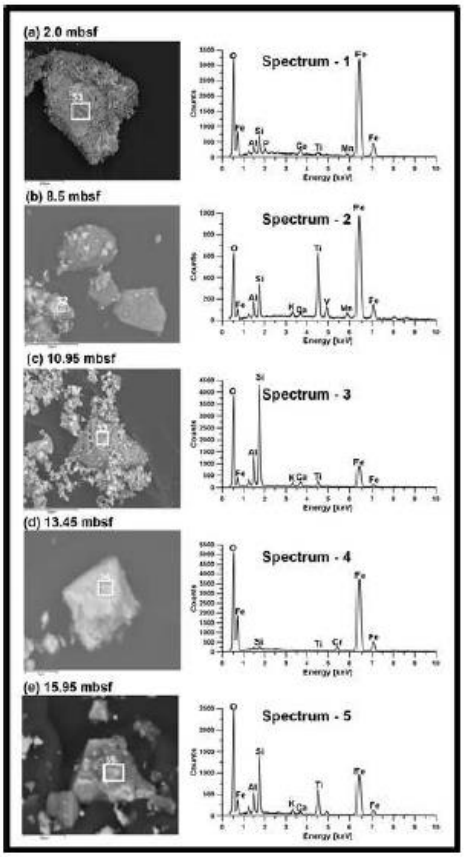
(a) 2.0 mbsf
Spectrum - 1
(b) 8.5 mbsf
Spectrum - 2
(c) 10.95 mbsf
Spectrum - 3
(d) 13.45 mbsf
Spectrum - 4
(e) 15.95 mbsf
Spectrum - 5

Figure -5

Figure - 6A

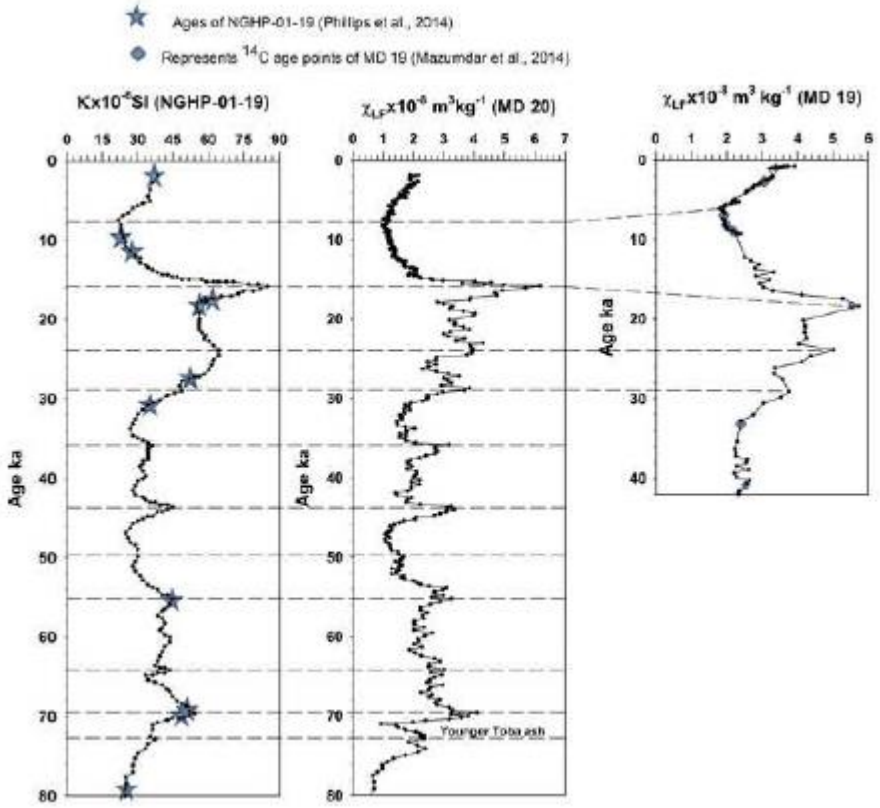
Ages of NGHP-01-19 (Phillips et al., 2014)
Represents ^{14}C age points of MD 19 (Mazumdar et al., 2014)
Kx10^{-6}SI (NGHP-01-19)
χ_{LF}x10^{-6} m^{3}kg^{-1} (MD 20)
χ_{LF}x10^{-8} m^3 kg^{-1} (MD 19)
Age ka
Younger Toba ash

Figure - 6B

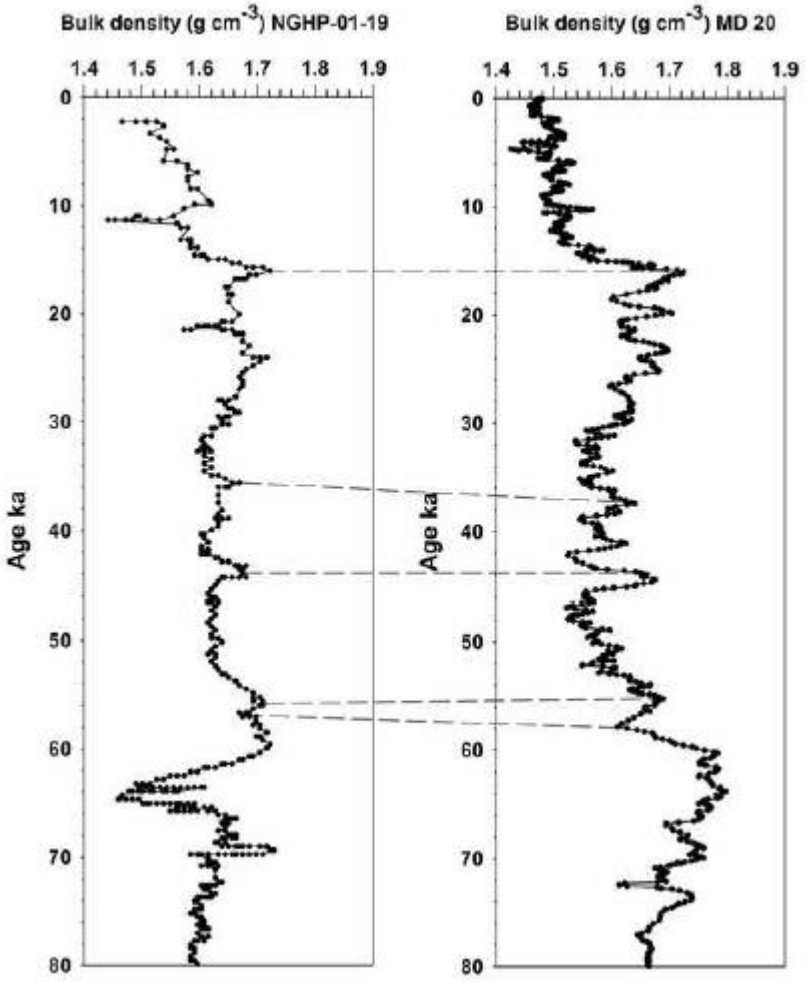
Bulk density (g cm-3) NGHP-01-19
Bulk density (g cm-3) MD 20
1.4 1.5 1.6 1.7 1.8 1.9
0 10 20 30 40 50 60 70 80
Age ka

Figure - 7A

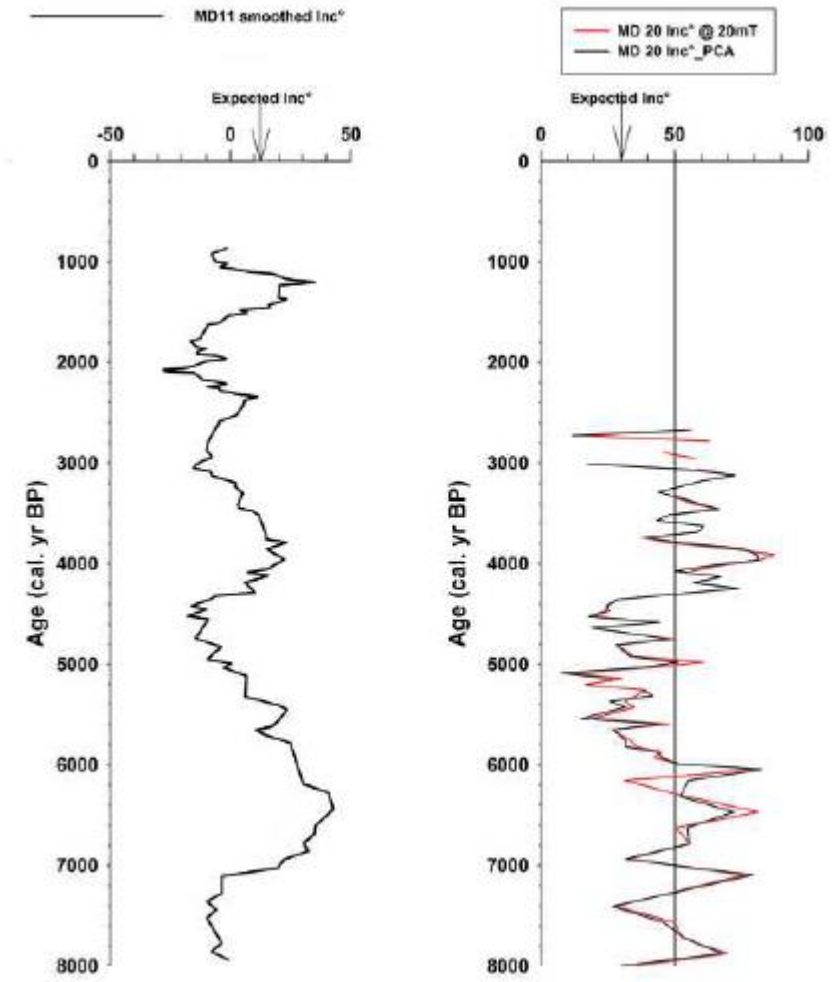
MD11 smoothed Inc°
Expected Inc°
-50
0
50
0
1000
2000
3000
4000
5000
6000
7000
8000
Age (cal. yr BP)
MD 20 Inc° @ 20mT
MD 20 Inc°_PCA
Expected Inc°
0
50
100
0
1000
2000
3000
4000
5000
6000
7000
8000
Age (cal. yr BP)

Figure - 7B

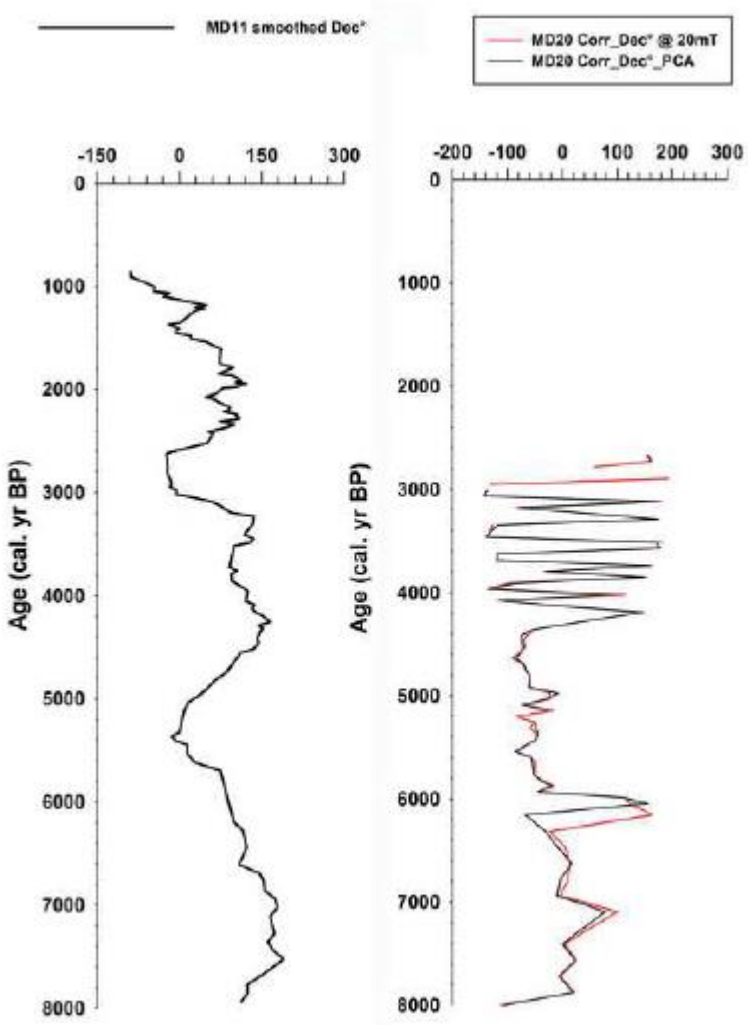
MD11 smoothed Dec*
MD29 Corr_Dec* @ 20mT
MD29 Corr_Dec*_PCA
-150
0
150
300
-200
-100
0
100
200
300
0
1000
2000
3000
4000
5000
6000
7000
8000
Age (cal. yr BP)

Figure - 8

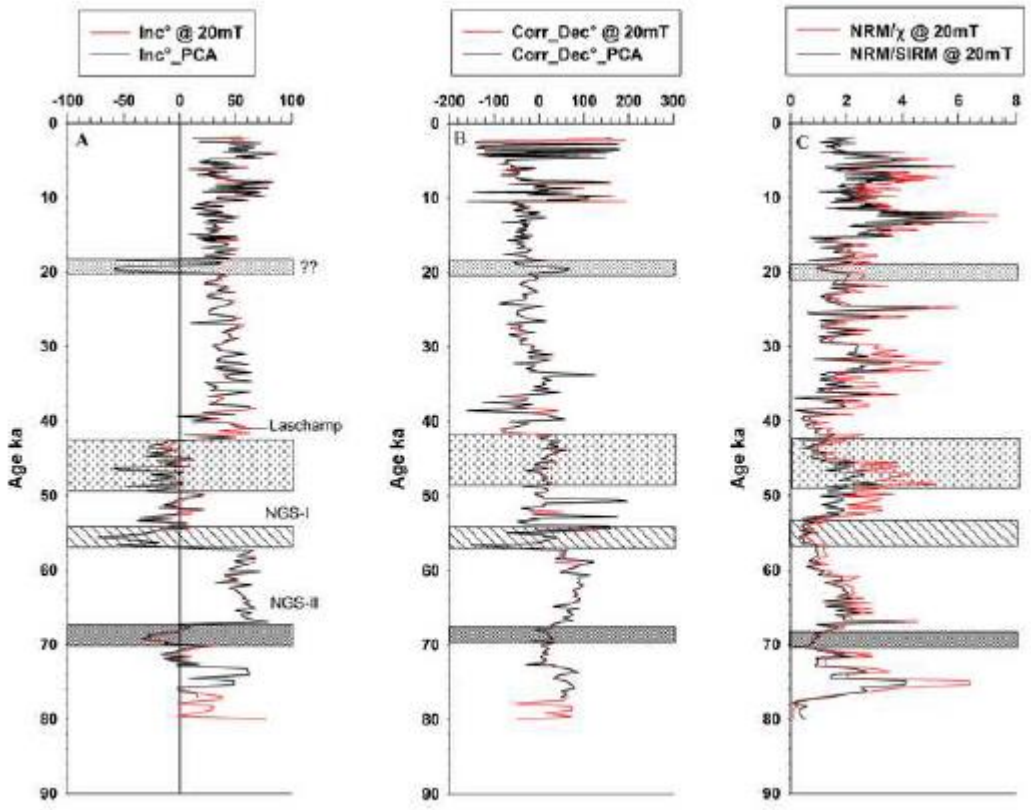
Inc° @ 20mT
Inc°_PCA
Corr_Dec° @ 20mT
Corr_Dec°_PCA
NRM/χ @ 20mT
NRM/SIRM @ 20mT
A
B
C
??
Laschamp
NGS-I
NGS-II
Age ka

Figure – 9

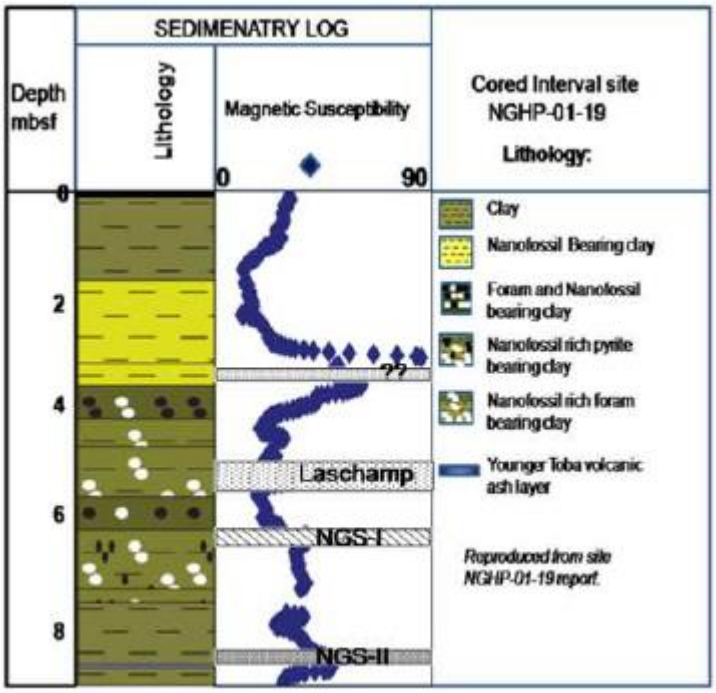
SEDIMENATRY LOG
Depth mbsf
Lithology
Magnetic Susceptibility
0
90
Cored Interval site NGHP-01-19
Lithology:
0
2
4
6
8
??
Laschamp
NGS-I
NGS-II
Clay
Nanofossil Bearing clay
Foram and Nanolossil bearing clay
Nanofossil rich pyrite bearing clay
Nanofossil rich foram bearing clay
Younger Toba volcanic ash layer
Reproduced from site NGHP-01-19 report.

Figure - 10

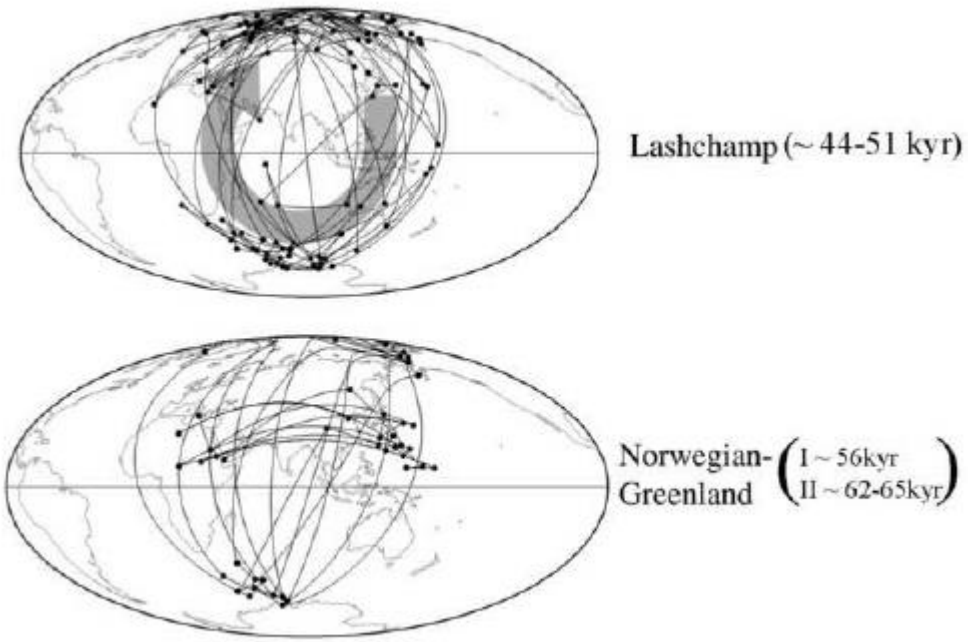

Table 1:

Depth (m)	Age ka	Inc° 20mT	Corr Dec°20mT	Inc° A	Corr Dec° A	Int/x	Int/sirm	MAD°
1.55	1.89	56.2	157.4	54.2	153.9	2.3	2.3	4.9
2	2.79	60.3	-83.5	60.4	-77.8	1.5	1.5	6.4
2.5	3.78	37.8	164.3	39.5	160.1	2.0	2.0	3.2
2.55	3.88	48.6	-33.0	52.6	-27.0	1.1	1.1	3.3
3.05	4.88	29.1	-50.8	28.5	-52.4	4.9	4.3	3.6
3.55	5.87	34.4	-58.5	33.2	-61.9	5.8	4.9	5.1
4	6.77	34.9	-48.0	31.5	-47.2	4.2	3.6	3.3
4.5	7.76	52.2	115.1	51.2	111.4	3.7	2.7	7.2
5.05	8.86	27.8	3.4	26.6	-0.3	3.9	2.8	1.2
5.5	9.75	76.6	168.8	72.1	156.9	3.8	3.2	4.4
5.55	9.85	74.9	81.1	74.2	86.5	2.5	2.0	4.1
6.05	10.85	24.3	-62.3	21.3	-58.7	3.2	2.9	1.1
6.5	11.74	22.3	-54.3	22.6	-57.5	3.8	3.2	2.5
7.05	12.84	44.7	-16.0	43.6	-19.4	5.8	5.4	1.8
7.5	13.73	33.1	-23.0	32.3	-24.9	2.7	2.3	1.6
8.05	14.83	28.7	-33.2	25.4	-33.4	3.1	2.4	1.4
8.5	15.72	34	-49.6	31.6	-51.1	1.5	1.2	2.2
9	18.41	-49.6	23.9	-57.2	14.1	0.8	0.6	1.1
9.5	21.29	30.3	-29.1	25.3	-33.4	1.9	1.6	1.5
10	24.18	47.2	-80.3	45.5	-88.8	2.0	1.7	1.8
10.5	27.16	57.5	-34.7	53	-39.0	1.2	1.1	2.7
11	29.87	30.2	-9.1	29.4	-12.9	3.2	2.4	2.9
11.5	32.16	53.2	-51.9	53.8	-57.6	5.4	3.6	2.5
12	34.45	47.7	28.2	46.9	24.3	1.6	1.1	1
12.55	37.21	35.5	-29.4	33	-31.0	2.5	1.9	16
13	39.70	36	52.1	28.6	56.9	0.6	0.4	5.6
13.55	42.75	-9.1	45.9	-10.4	45.7	2.0	1.4	3.2
14	44.98	9.4	8.1	7.8	4.7	1.2	0.8	1.1
14.5	47.30	-20.9	11.7	-25.5	10.9	4.2	2.6	0.8
15	49.62	-4.8	-9.1	-8.8	-7.1	2.4	1.4	3
15.5	51.87	22.5	-12.4	19.6	-12.7	3.3	1.9	4.3
16	54.10	-8.3	156.9	-10.1	156.3	0.6	0.5	3.4
16.55	57.37	62.4	59.6	65.8	62.7	1.2	0.9	1.4
17	60.60	49	113.7	41	112.9	1.3	1.0	3.3
17.5	64.18	61.2	90.8	62.2	80.7	1.3	1.2	1.2
18	67.34	2.9	31.6	-1	27.2	1.0	0.9	3.4
18.5	70.17	32.6	6.3	25.9	3.8	0.7	0.7	3
19	72.22	-8.5	8.2	-10.8	7.2	1.2	0.9	3
19.5	75.79	1	77.0	-2.4	80.1	4.0	2.5	14.4
20	80.00	77.1	-49.6	16.8	60.7	0.1	0.5	27.7

Table2:

Depth (m)	χ_{LF}x10^{-8} m^{3}kg^{-1}	χ_{ARM}x10^{-5} m^{3}kg^{-1}	SIRMx10^{-5} Am^{2}kg^{-1}	χ_{FD} (%)	χ_{ARM}/SIRM mA^{-1}x10^{-3}	SIRM/χ_{LF} Am^{-1}	Soft-IRMx10^{-5}Am^{2}kg^{-1}	Hard-IRMx10^{-5} Am^{2}kg^{-1}	S-ratio
1.5	1.89	0.35	183.0	7.4	1.9	9.7	152.9	11.8	0.935
2	2.05	0.41	208.1	6.9	2	10.2	184.4	14.3	0.932
2.5	1.67	0.33	174.1	6.1	1.9	10.4	140.7	11.3	0.935
3	1.52	0.34	170.6	6.4	2	11.2	136.0	14.5	0.915
3.5	1.19	0.31	152.3	5.7	2.1	12.8	120.1	13.4	0.912
4	1.35	0.34	160.5	6.8	2.1	11.9	121.1	14.2	0.912
4.5	1.12	0.33	153.4	5.1	2.1	13.7	109.5	13.3	0.913
5	1.14	0.36	152.2	5.9	2.4	13.3	108.7	12.7	0.917
5.5	1.25	0.36	149.0	5.5	2.4	11.9	107.2	13.0	0.913
6	1.28	0.35	145.5	4.4	2.4	11.3	98.5	12.2	0.916
6.5	1.33	0.35	159.5	5.7	2.2	12.0	119.7	13.0	0.919
7	1.75	0.39	179.9	6.8	2.2	10.3	135.1	16.3	0.909
7.5	2.11	0.50	246.8	6.2	2	11.7	206.2	17.9	0.927
8	2.20	0.50	267.1	5.8	1.9	12.1	227.1	22.0	0.918
8.5	4.98	0.67	585.0	6.4	1.1	11.7	532.5	33.8	0.942
9	3.29	0.55	424.1	7.1	1.3	12.9	354.3	24.5	0.942
9.5	3.86	0.63	460.5	6.7	1.4	11.9	424.4	26.8	0.942
10	3.93	0.58	469.6	6.2	1.2	12.0	447.6	26.4	0.944
10.5	3.50	0.60	383.2	9.1	1.6	10.9	362.0	21.0	0.945
11	2.47	0.52	331.3	7.3	1.6	13.4	287.5	18.9	0.943
11.5	1.57	0.40	236.2	2.7	1.7	15.1	187.1	16.7	0.929
12	1.56	0.44	231.6	3.1	1.9	14.8	175.8	12.7	0.945
12.5	2.71	0.50	367.8	4.2	1.4	13.6	304.9	21.0	0.943
13	2.07	0.47	312.5	6.3	1.5	15.1	249.5	17.8	0.943
13.5	1.95	0.44	265.2	5.3	1.6	13.6	219.8	19.8	0.925
14	2.10	0.49	325.1	2.8	1.5	15.5	244.9	22.1	0.932
14.5	1.14	0.33	186.3	1.2	1.8	16.3	123.9	17.8	0.905
15	1.52	0.41	250.1	5.5	1.6	16.5	165.0	21.9	0.912
15.5	1.44	0.51	248.6	4.8	2.1	17.2	155.7	17.6	0.929
16	2.97	0.59	396.4	6.1	1.5	13.3	335.9	24.1	0.939
16.5	2.45	0.48	308.6	5.6	1.6	12.6	236.7	22.9	0.926
17	2.17	0.40	280.2	3.5	1.4	12.9	249.6	19.8	0.929
17.5	3.02	0.51	337.5	5.8	1.5	11.2	304.5	24.5	0.927
18	2.61	0.47	282.1	8.2	1.7	10.8	230.1	22.5	0.920
18.5	3.57	0.65	379.7	6.7	1.7	10.6	352.6	18.2	0.952
19	2.21	0.57	284.9	5.7	2	12.9	214.6	19.1	0.933
19.5	1.15	0.39	180.3	4.0	2.2	15.7	112.9	15.0	0.917
20	0.63	0.01	29.4	5.0	0.3	4.7	24.2	4.9	0.834
19.5	1.15	0.39	180.3	4.0	2.2	15.7	112.9	15.0	0.917
20	0.63	0.01	29.4	5.0	0.3	4.7	24.2	4.9	0.834